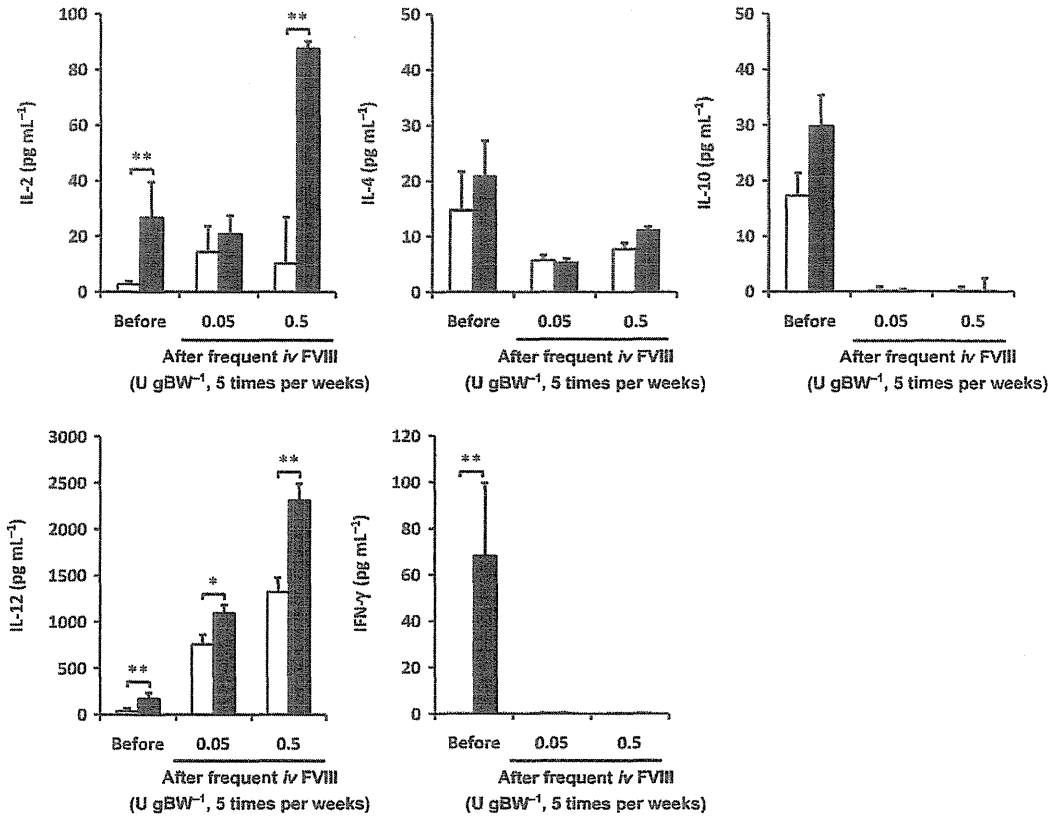

Fig. 6. Effect of serial infusion of FVIII on cytokine response of pre-immunized haemophilia A mice. Haemophilia A mice were intravenously immunized with 0.05 U g^{-1} BW FVIII at 16, 18, 20, 22 and 24 weeks. After measurement of anti-FVIII inhibitory antibodies titers, preimmunized mice were frequently administered with FVIII (0.05 or 0.5 U g^{-1} BW five times per week) through iVAD system. Splenocytes from pre-immunized (before, $n = 5$), frequently FVIII-infused [0.05 ($n = 4$) or 0.5 ($n = 3$) U g^{-1} BW five times per week] mice were cultured in the absence (open bars) or presence (closed bars) of 3 nM FVIII, and their cytokine production (IL-2, IL-4, IL-10, IL-12 and IFN-γ) were analyzed by ELISA as described in Methods. Values (pg mL^{-1}) are means ± SD. $^{*}P < 0.05$; $^{**}P < 0.03$.

IL-2, IL-12 and IFN-γ in response to *in vitro* FVIII stimulation (Fig. 6). In contrast, splenocytes deriving from mice with serial infusion of 0.05 U g^{-1} BW FVIII did not increase their production of IL-2 and IFN-γ, although they could secrete IL-12 after addition of FVIII. Moreover, 0.5 U g^{-1} BW FVIII-repeated administrated mice produced significant amounts of IL-2 and IL-12, but did not change IFN-γ levels even after stimulation of FVIII.

Discussion

Haemophilia A patients with inhibitors are infused daily FVIII according to immune tolerance protocols with the aim of eradicating the antibody [10,11]. Central VADs have been used to facilitate repeated administration of clotting factor concentrates in haemophiliac children requiring ITI [12,13]. We here established a method to implant a VAD into haemophilia A mice (Fig. 1). We could prevent exposure to FVIII antigen in the mice during the surgical procedure, because it is known that the innate immune system is activated by endogenous 'danger signals' such as tissue damage that involves necrotic cell death [14]. Indeed, titers of anti-FVIII inhibitory antibodies of the mice were elevated up to 400 BU mL^{-1} after the fifth intermittent stimulation of FVIII, in good agreement with previous findings [9]. Central VADs are associated with infectious and thrombotic complications necessitating the removal [6], although recent data from the international-ITI study showed that infectious episodes during ITI may not influence treatment outcome [15]. In our animal models, one mouse that had been frequently administered 0.05 U g^{-1} BW of FVIII exhibited a catheter-related bleeding (Fig. 2; LD#3), whereas another one with 0.5 U g^{-1} BW of FVIII had occlusion of iVAD system (Fig. 2, HD#4). Nonetheless, the iVAD would be a useful tool to evaluate immune response against sequential infusion of FVIII antigen in haemophilia A mice because they could be repeatedly infused more than 180 times over 50 weeks.

Recent study showed that port systems are suitable for inhibitor-expressing children with good predictors of ITI success [16,17]. In our murine model, high titers against FVIII (>2000 BU mL^{-1} during 50–100 EDs) were decreased to <500 BU mL^{-1} after 130–150 EDs in all

mice with serial infusion of 0.05 U g^{-1} BW of FVIII, even though they were continually exposed to FVIII antigen (Fig. 2). In contrast, mice administered high-dose 0.5 U g^{-1} BW FVIII five times a week had high titers of anti-FVIII inhibitory antibodies over 180 EDs, suggesting that dose of FVIII antigen might be crucial for the immune response in haemophilia A mice. We could not induce immune tolerance in any adult haemophilia A mouse with sequential infusion of FVIII antigen, according to the international consensus in which successful immune tolerance induction in haemophilia A is currently defined as both an undetectable inhibitor titer (less than or equal to 0.6 BU mL^{-1}) and normalized FVIII pharmacokinetics [18]. However, anti-FVIII IgG titers were markedly decreased to undetectable levels after 80–180 EDs in mice with serial infusion of 0.05 U mL^{-1} FVIII (Fig. 3). The discrepancy between anti-FVIII inhibitory titers and anti-FVIII IgG titers may be dependent on assay methods in which the former was one-stage APTT measurement and the latter was ELISA using an anti-FVIII monoclonal antibody as standard.

In haemophilia A patients, several researchers reported that IgG4 is the major component of anti-FVIII antibodies, although all IgG subclasses have been found [19,20]. In murine models, we showed that kinetics of anti-FVIII IgG1, IgG2a and IgG2b titers of haemophilia A mice with serial infusion of 0.05 U g^{-1} BW FVIII were similar to those administered 0.5 U g^{-1} BW FVIII (Fig. 4). In contrast, titers of anti-FVIII IgG3 subclass were decreased after 50–100 EDs in mice with serial infusion of 0.05 U g^{-1} BW FVIII. The Th1 immune response is believed predominant in patients with inhibitors in the long term [21], and was also the predominant response in mice that developed antibodies after challenge in adulthood [22,23]. We demonstrated a dose-dependent $CD4^+$ T-cell proliferative response to FVIII in preimmunized mice (five times injection of FVIII every 2 weeks), which is compatible with previous studies demonstrating that human FVIII is highly immunogenic in haemophiliac mice (Fig. 5) [24]. Interestingly, we observed that haemophilia A mice with sequential infusion of 0.05 U g^{-1} BW FVIII after 180 EDs failed to develop $CD4^+$ T-cell proliferative response to *in vitro* stimulation of FVIII antigen (Fig. 5). These T cells could not produce any IL-2, IL-4, IL-10, nor IFN-γ (Fig. 6), whereas those from mice immunized with five-times infusion of 0.5 U g^{-1} BW FVIII were able to secrete significant amounts of IL-2, IL-12 and IFN-γ. It is known that Th1 cells are initiators of antibody responses, and that they participate in class switching by releasing IFN-γ, which preferentially induces IgG2a and IgG3 in mouse [25]. Consequently, the FVIII-specific Th1 cytokine response may be partially suppressed by serial administration of FVIII in haemophilia A mice with inhibitors.

Several potential mechanisms of ITI have been identified [26]. These include clonal deletion (i.e. removal of immune-response cells through programmed cell death or apoptosis), anergy (failure of immune cells to respond to the FVIII molecule), or ignorance (i.e. the immune-response cells are 'blind' to the presence of FVIII). Our data suggest that sequential exposure of FVIII antigen could partially block anti-FVIII inhibitory antibody production, inducing T-cell anergy in haemophilia A mice with inhibitor, although our murine ITI model against heteroantibodies is fundamentally different from human ITI therapy against alloantibodies. However, further evaluation using completely continuous infusion system for the exposure of FVIII antigen will be necessary to confirm its efficacy in inducing immune tolerance [27]. Furthermore, understanding of the underlying mechanisms of immune tolerance induced by serial administration of FVIII is essential for the development of this strategy for haemophilia A patients with inhibitors.

Acknowledgement

We thank D.V.M. Hisae Yamauchi, D.V.M. Akane Hirosawa and Ms. Chizuko Nakamikawa for their excellent technical assistance. This work was supported in part by a Grant-in-Aid for Scientific Research (#19591133, #20591155, #21790920 and #21591249) from the Ministry of Education, Culture, Sports, Science and Technology, and by a Health and Labor Sciences Research Grant for Research from the Ministry of Health, Labor and Welfare, by Support Program for Strategic Research Platform, Baxter Hemophilia Scientific Research & Education Fund, and by JKA promotion funds from KEIRIN RACE.

Author contributions

SM designed and performed the research, analyzed data and wrote the paper; EK, YK, AY and AS performed experiments; SM, TO, JM and YS analyzed data and revised the paper.

Disclosures

The authors stated that they had no interests which might be perceived as posing a conflict or bias.

References

1 Hoyer LW. Hemophilia A. *N Engl J Med* 1994; 330: 38–47.
2 Ehrenforth S, Kreuz W, Scharrer I *et al.* Incidence of development of factor VIII and factor IX inhibitors in haemophiliacs. *Lancet* 1992; 339: 594–8.
3 Hoyer LW. Why do so many haemophilia A patients develop an inhibitor? *Br J Haematol* 1995; 90: 498–501.
4 Kreuz W, Becker S, Lenz E *et al.* Factor VIII inhibitors in patients with hemophilia A: epidemiology of inhibitor development and induction of immune tolerance for factor VIII. *Semin Thromb Hemost* 1995; 21: 382–9.
5 Ewenstein BM, Valentino LA, Journeycake JM *et al.* Consensus recommendations for use of central venous access devices in haemophilia. *Haemophilia* 2004; 10: 629–48.
6 Valentino LA, Ewenstein B, Navickis RJ, Wilkes MM. Central venous access devices in haemophilia. *Haemophilia* 2004; 10: 134–46.

7 Santagostino E, Mancuso ME. Venous access in haemophilic children: choice and management. *Haemophilia* 2010; 16(Suppl 1): 20–4.

8 Bi L, Lawler AM, Antonarakis SE, High KA, Gearhart JD, Kazazian HH Jr. Targeted disruption of the mouse factor VIII gene produces a model of haemophilia A. *Nat Genet* 1995; 10: 119–21.

9 Madoiwa S, Yamauchi T, Hakamata Y *et al.* Induction of immune tolerance by neonatal intravenous injection of human factor VIII in murine hemophilia A. *J Thromb Haemost* 2004; 2: 754–62.

10 Brackmann HH. Induced immunotolerance in factor VIII inhibitor patients. *Prog Clin Biol Res* 1984; 150: 181–95.

11 Nilsson IM, Berntorp E, Zettervall O. Induction of immune tolerance in patients with hemophilia and antibodies to factor VIII by combined treatment with intravenous IgG, cyclophosphamide, and factor VIII. *N Engl J Med* 1988; 318: 947–50.

12 Liesner RJ, Vora AJ, Hann IM, Lilleymann JS. Use of central venous catheters in children with severe congenital coagulopathy. *Br J Haematol* 1995; 91: 203–7.

13 Santagostino E, Gringeri A, Muca-Perja M, Mannucci PM. A prospective clinical trial of implantable central venous access in children with haemophilia. *Br J Haematol* 1998; 102: 1224–8.

14 Kono H, Rock KL. How dying cells alert the immune system to danger. *Nat Rev Immunol* 2008; 8: 279–89.

15 DiMichele DM, Goldberg I, Foulkes M, Hay RM. International prospective randomized immune tolerance (ITI) study: preliminary results of therapeutic efficacy and safety. *Haemophilia* 2010; 16(Suppl 4): 29.

16 DiMichele DM, Hoots WK, Pipe SW, Rivard GE, Santagostino E. International workshop on immune tolerance induction: consensus recommendations. *Haemophilia* 2007; 13(Suppl 1): 1–22.

17 Mancuso ME, Mannucci PM, Sartori A, Agliardi A, Santagostino E. Feasibility of prophylaxis and immune tolerance induction regimens in haemophilic children using fully implantable central venous catheters. *Br J Haematol* 2008; 141: 689–95.

18 Astermark J, Morado M, Rocino A *et al.* Current European practice in immune tolerance induction therapy in patients with haemophilia and inhibitors. *Haemophilia* 2006; 12: 363–71.

19 Fulcher CA, de Graaf Mahoney S, Zimmerman TS. FVIII inhibitor IgG subclass and FVIII polypeptide specificity determined by immunoblotting. *Blood* 1987; 69: 1475–80.

20 Gilles JG, Arnout J, Vermylen J, Saint-Remy JM. Anti-factor VIII antibodies of hemophiliac patients are frequently directed towards nonfunctional determinants and do not exhibit isotypic restriction. *Blood* 1993; 82: 2452–61.

21 Reding MT, Lei S, Lei H, Green D, Gill J, Conti-Fine BM. Distribution of Th1- and Th2-induced anti-factor VIII IgG subclasses in congenital and acquired hemophilia patients. *Thromb Haemost* 2002; 88: 568–75.

22 Wu H, Reding M, Qian J *et al.* Mechanism of the immune response to human factor VIII in murine hemophilia A. *Thromb Haemost* 2001; 85: 125–33.

23 Sasgary M, Ahmad RU, Schwarz HP, Turecek PL, Reipert BM. Single cell analysis of factor VIII-specific T cells in hemophilic mice after treatment with human factor VIII. *Thromb Haemost* 2002; 87: 266–72.

24 Qian J, Borovok M, Bi L, Kazazian HH Jr, Hoyer LW. Inhibitor antibody development and T cell response to human factor VIII in murine hemophilia A. *Thromb Haemost* 1999; 81: 240–4.

25 Stavnezer J. Immunoglobulin class switching. *Curr Opin Immunol* 1996; 8: 199–205.

26 Behrmann M, Pasi J, Saint-Remy JM, Kotitschke R, Kloft M. Von Willebrand factor modulates factor VIII immunogenicity: comparative study of different factor VIII concentrates in a haemophilia A mouse model. *Thromb Haemost* 2002; 88: 221–9.

27 Abe C, Tashiro T, Tanaka K, Ogihara R, Morita H. A novel type of implantable and programmable infusion pump for small laboratory animals. *J Pharmacol Toxicol Methods* 2009; 59: 7–12.

Cancer Research

NF-κB Activity Regulates Mesenchymal Stem Cell Accumulation at Tumor Sites

Ryosuke Uchibori[1], Tomonori Tsukahara[1], Hiroyuki Mizuguchi[4], Yasushi Saga[2], Masashi Urabe[1], Hiroaki Mizukami[1], Akihiro Kume[1], and Keiya Ozawa[1,3]

Abstract

Mesenchymal stem cells (MSC) accumulate at tumor sites when injected into tumor-bearing mice, perhaps offering cellular vectors for cancer-targeted gene therapy. However, the molecular mechanisms involved in MSC targeting the tumors are presently little understood. We focused on MSC–endothelial cell (EC) adhesion following TNF-α stimulation in an attempt to elucidate these mechanisms. Interestingly, stimulation of MSCs with TNF-α enhanced the adhesion of MSCs to endothelial cells *in vitro*. This adhesion was partially inhibited by blocking antibodies against vascular cell adhesion molecule-1 (VCAM-1) and very late antigen-4 (VLA-4). It is well known that TNF-α induces VCAM-1 expression via the NF-κB signaling pathway. Parthenolide has an anti-inflammatory activity and suppressed NF-κB activity by inhibition of IκBα phosphorylation after TNF-α stimulation and strongly inhibited TNF-α–induced VCAM-1 expression on MSCs. *In vivo* imaging using luciferase-expressing MSCs revealed that the bioluminescent signal gradually increased at tumor sites in mice injected with untreated MSCs. In contrast, we observed very weak signals at tumor sites in mice injected with parthenolide-treated MSCs. Our results suggest that NF-κB activity regulates MSC accumulation at tumors, by inducing VCAM-1 and thereby its interaction with tumor vessel endothelial cells. These findings have implications for the ongoing development of efficient MSC-based gene therapies for cancer treatment. *Cancer Res; 73(1); 364–72. ©2012 AACR.*

Introduction

Mesenchymal stem cells (MSC) are nonhematopoietic stem cells with high-proliferative potency and have the ability to differentiate into multiple lineages. They are detected in several adult and fetal tissues, including bone marrow, adipose tissue, and umbilical cord blood. MSCs have generated a great deal of interest in their potential use in regenerative medicine due to their ability to migrate to damaged tissues and to produce cytokines. Furthermore, MSCs can be easily genetically modified with viral vectors to be used as novel cellular vehicles in gene therapy protocols. MSCs are also used to treat severe acute GVHD, because they accumulate at inflammatory lesions and have immunomodulatory activity.

Interestingly, recent studies indicated that MSCs also have the ability to accumulate in tumors. Therefore, they can be used as cellular vehicles for cancer-targeted gene therapy. Intravenous injection of engineered MSCs expressing IFN-β was reported to inhibit the growth of melanoma pulmonary metastasis (1) and breast cancer (2) in mice and also prolonged the survival of mice with glioma xenografts (3). Furthermore, interleukin (IL)-12, which improves immune surveillance against cancer cells (4), and chemokine CX3CL1 (fractalkine), which is able to activate T cells and natural killer (NK) cells (5), were used as therapeutic molecules. We have also shown that retrovirus vector–producing MSCs also effectively inhibit tumor growth (6). In this context, treatment has been developed using retroviral vectors expressing the thymidine kinase of herpes simplex virus combined with the prodrug ganciclovir.

The ability of MSCs to specifically localize the multiple tumors, makes them extremely attractive for targeted cancer therapy. The most likely cause of preferential migration was considered to be the release of chemotactic gradients from tumor tissues. MSCs have a variety of chemokine and cytokine receptors and respond functionally to ligands *in vitro*. Tumors are known to produce a large amount of chemokines and cytokines, which could serve as ligands for the receptors on MSCs (7). Therefore, the mechanism of MSC accumulation at the site of tumors seems to be based on their migratory ability. Nevertheless, although various growth factors and chemokines, such as platelet-derived growth factor (PDGF), hepatocyte growth factor (HGF), and stromal cell–derived factor-1α (SDF-1α) may be involved, the detailed molecular mechanisms of MSC accumulation at tumors are poorly understood.

Authors' Affiliations: [1]Division of Genetic Therapeutics, Center for Molecular Medicine; [2]Department of Obstetrics and Gynecology; [3]Division of Hematology, Department of Medicine, Jichi Medical University, Tochigi; and [4]Department of Biochemistry and Molecular Biology, Osaka University, Osaka, Japan

Note: Supplementary data for this article are available at Cancer Research Online (http://cancerres.aacrjournals.org/).

Corresponding Author: Keiya Ozawa, Division of Genetic Therapeutics, Center for Molecular Medicine, Jichi Medical University, 3311-1 Yakushiji, Shimotsuke, Tochigi 329-0498, Japan. Phone: 81-285-58-7402; Fax: 81-285-44-8675; E-mail: kozawa@jichi.ac.jp

doi: 10.1158/0008-5472.CAN-12-0088

In the present study, we focused on MSC–endothelial cell (EC) adhesion following TNF-α stimulation in an attempt to elucidate the mechanism of MSC accumulation at tumors.

Materials and Methods

Cell culture

Bone marrow–derived human MSCs (Lonza Walkersville, Inc.) were cultured in mesenPRO RS medium (Invitrogen). HEK293-derived AD-293 cells (Stratagene), human embryonic fibroblasts WI-38 (RIKEN BRC), human colon adenocarcinoma cell lines SW480 (Cell Resource Center for Biomedical Research Institute of Development, Aging and Cancer, Tohoku University, Miyagi, Japan), and SW480/RFP that was generated by transduction of SW480 with red fluorescent protein-expressing retrovirus vectors (RV-RFP), were grown in Dulbecco's Modified Eagle's Medium (DMEM)/F-12 medium (Invitrogen) supplemented with 10% FBS, 100 U/mL penicillin, and 100 μg/mL streptomycin (P/S). Human endothelial progenitor cells (ApproCell Inc.) were cultured in endothelial progenitor cells grown medium (ApproCell Inc.). Human colon adenocarcinoma cell lines Colo205 (Cell Resource Center for Biomedical Research Institute of Development, Aging and Cancer Tohoku University) and Colo205/RFP that was generated by transduction with RV-RFP, were grown in RPMI medium (Invitrogen) supplemented with FBS and P/S. All cultures were kept in an incubator at 37°C and 5% CO_2.

Adenoviral vectors

Adenoviral vectors expressing a GFP were constructed by an improved *in vitro* ligation method (8, 9). The shuttle plasmid pHMCA5-GFP contains a CA promoter (a β-actin promoter/CMV enhancer with a β-actin intron), *GFP* gene, and a bovine growth hormone (BGH) polyadenylation signal, all of which are flanked by I-CeuI and PI-SceI restriction sites. I-CeuI/PI-SceI–digested pHMCA5-GFP was ligated with I-CeuI/PI-SceI–digested pAdHM4, resulting in pAdHM4-CAGFP. pAdHM41-K7-CAGFP was constructed by ligation of I-CeuI/PISceI–digested pHMCA5-GFP with I-CeuI/PI-SceI–digested pAdHM41-K7 (10). Viruses (Ad5-GFP and AdK7-GFP) were generated by transfection of PacI-digested pAdHM4-CAGFP and pAdHM41-K7-CAGFP, respectively, into AD-293 cells with SuperFect (Qiagen) according to the manufacturer's instructions. Each virus was purified by $CsCl_2$ step gradient ultracentrifugation followed by $CsCl_2$ linear gradient ultracentrifugation. Virus particles and biologic titers of each vector preparation were determined as described by Mittereder and colleagues (11). We also created Ad vectors expressing luciferase (Luc) using the shuttle plasmid pHMCA5-Luc, which contains the *Luc* gene derived from pELuc-test (Toyobo Co. Ltd.). MSCs and fibroblasts were seeded in culture plates or flasks at a density of 1×10^4 cells/cm^2, and the next day the cells were treated with each adenovirus vector for 1.5 hours. The medium containing the vectors was removed and replaced with fresh medium.

Animal models

All animal experiments were approved by the Jichi Medical University (Tochigi, Japan) ethics committee and carried out in accordance with the NIH Guide for the Care and Use of Laboratory Animals. To create tumor-bearing mice, SW480/RFP cells (3×10^6) were subcutaneously inoculated into 4- to 6-week-old male Balb/c nu/nu mice (Clea Japan Inc.). The mice were used for experiments 7 days after inoculation.

Immunohistochemistry

Cultured MSCs and fibroblasts were transduced with AdK7-GFP at a concentration of 3,000 virus particles per cell (vp/cell). Two days after transduction, cells were injected into the left ventricular cavities (1×10^6, day 0) of tumor-bearing mice. Mice were sacrificed on day 4, and 7-μm serial cryosections from frozen tissues were processed. Immunohistochemistry was conducted with fluorescein isothiocyanate (FITC)-conjugated anti-GFP antibody (ab6662; Abcam Inc.) on tumor cryosections to detect MSCs or fibroblasts. Nuclei were stained with 4′,6-diamidino-2-phenylindole (DAPI; Vector Laboratories, Inc.). Images were obtained with a fluorescence microscope (BZ-9000; Keyence). SW480/RFP cells (3×10^6) were subcutaneously inoculated into 4- to 6-week-old male Balb/c nu/nu mice. Mice were sacrificed on day 11, serial sections from tumor tissues were processed. Immunohistochemistry was conducted with anti-mouse CD34 monoclonal antibody (MEC14.7; GeneTex Inc.) on tumor section to detect tumor blood vessels. Histofine Simple Stain Mouse MAX PO (Nichirei Biosciences, Inc.) was used as a horseradish peroxidase–conjugated secondary antibody, and 3,3′-diaminobenzidine (DAB) solution was used for brown color development. Sections were then counterstained with Hematoxylin (Wako Pure Chemical Industries, Ltd.). Images were obtained with a fluorescence microscope (BZ-9000).

In vivo imaging of homing ability to tumors

Cultured MSCs and fibroblasts were transduced with AdK7-Luc at a concentration of 3,000 and 680 vp/cell, respectively. Two days after transduction, cells were injected into the left ventricular cavities (1×10^6, day 0) of tumor-bearing mice, and then optical bioluminescence imaging was conducted to periodically trace the cells using an *in vivo* imaging system (IVIS; Xenogen). To detect bioluminescence from MSCs or fibroblasts, the reporter substrate D-luciferin (Ieda Chemical Co., Ltd.) was injected into the mouse peritoneum (75 mg/kg body weight) for scanning. The luminescent intensity at tumor sites was analyzed using Living Image software (Xenogen).

In vitro migration assays

Cultured MSCs or fibroblasts were serum-starved for 12 hours. One hundred microliters of tumor conditioning medium (CM), or serum-free medium supplemented with PDGF-BB (10 ng/mL), HGF (30 ng/mL), fibroblast growth factor-β (FGF-β; 20 ng/mL), SDF-1α (150 ng/mL), VEGF-A (25 ng/mL), or monocyte chemoattractant protein-1 (MCP-1; 100 ng/mL) was added to the lower wells of migration chambers (8-μm pore size; Neuro Probe, Inc.); MSCs or fibroblasts (4×10^4) were added to the upper wells. All recombinant proteins were purchased from R&D systems Inc.. Medium alone (DMEM/F-12) was used as a negative control and treatment with 30% FBS was the positive control. After incubation for 24 hours at

37°C, cells were labeled with CyQUANT NF dye, and cells attached to the lower surface of the filters were detached with trypsin. Fluorescent intensity was measured using a fluoroscan, and the number of adherent cells was quantified using a standard curve constructed by a known number of cells.

Flow cytometric analysis of adhesion molecules

Cultured MSCs, fibroblasts or endothelial cells were stimulated with TNF-α and harvested by trypsinization. Cell aliquots were incubated with FITC-conjugated monoclonal antibodies (BD) against vascular cell adhesion molecule-1 (VCAM-1), CD49d, CD29 (Integrin-β1), and analyzed by flow cytometry (FACScan; BD Biosciences). For each analysis, an aliquot of cells was also stained with isotype control immunoglobulin G (IgG)–conjugated to FITC as a negative control.

Assay for TNF-α produced in tumor-bearing mice

SW480/RFP (3×10^6) cells were subcutaneously inoculated into nude mice. Seven days after inoculation, mice were anesthetized with an overdose of isoflurane inhalation. The blood was collected and allowed to coagulate overnight on ice. After centrifugation of the samples (2,000 × *g*, 30 minutes, 4°C), the serum was removed and stored at −70°C. Tumor, spleen, and liver tissues were homogenized in 1.5 mL of α-minimum essential medium using a tissue homogenizer. The homogenates were then centrifuged (2,000 × *g*, 30 minutes, 4°C), and the supernatant was removed and recentrifuged (14,000 × *g*, 30 minutes, 4°C). Serum and supernatants from tissue homogenates were kept at −70°C until use. TNF-α was assayed using a commercially available ELISA kit (mouse TNF-α Instant ELISA; Bender MedSystems) according to the manufacturer's protocols.

***In vitro* adhesion assays**

For adhesion assays, endothelial cells (at 4 passages) were cultured to confluence on fibronectin-coated 96-well plates (20 ng/mL; Sigma-Aldrich, Inc.) and treated with TNF-α (10 ng/mL) for 12 hours before assaying. MSCs and fibroblasts were treated with TNF-α (10 ng/mL) 12 hours before the adhesion assays and incubated with isotype control IgG or anti-VCAM-1 or very late antigen-4 (VLA-4; 10 μg/mL) monoclonal antibodies (mAb) for 1 hour. Cells were labeled with CyQUANT NF dye, and 1×10^4 cells were seeded onto endothelial cells. After 30 minutes of incubation at 37°C, wells were washed thoroughly 3 times with PBS to remove nonadherent cells. Fluorescent intensity was measured using a fluoroscan, and the number of adherent cells was quantified using a standard curve constructed by a known number of cells. In some experiments, MSCs and fibroblasts were pretreated for adhesion studies with one of the following substances: TNF-α (10 ng/mL), anti-VCAM-1 antibody (mouse monoclonal anti-rat, clone 5F10, 10 μg/mL, Eurogentec), or anti-VLA-4 antibody (mouse monoclonal anti-rat, clone 1A29, 10 μg/mL, Research Diagnostics).

Parthenolide treatment of MSCs

Parthenolide (Biomol) was reconstituted in dimethyl sulfoxide (DMSO; Sigma-Aldrich, Inc.) to a stock concentration of 0.4 mol/L and subsequently diluted in PBS. MSCs were treated with parthenolide (5 μmol/L) for 6 hours before experiments. To assess the effect of parthenolide treatment of transgene expression, cells were reseeded into 96-well plates, and luciferase assays were conducted using luciferase-expressing MSCs. Cell viability after parthenolide treatment was also examined with Cell Proliferation Kit II [2,3-bis[2-methoxy-4-nitro-S-sulfophenynl]H-tetrazolium-5 carboxanilide inner salt (XTT); Roche Diagnostics GmbH] according to the manufacturer's instructions.

Western blotting

Western blot analysis was conducted to measure the NF-κB pathways. Next, MSCs were pretreated with parthenolide or vehicle (DMSO) for 6 hours, and then cultured with TNF-α (10 ng/mL) for 3 minutes. Cells were lysed in radioimmunoprecipitation assay (RIPA) buffer containing protease inhibitor (Pierce Biotechnology). Protein extracts were electrophoresed on a 4% to 12% Bis–Tris gel (Invitrogen), and transferred to polyvinylidene difluoride (PVDF) membranes. Membranes were incubated in PVDF blocking reagent (TOYOBO), and then incubated with primary antibodies against the following proteins: IκBα, phospho-IκBα (Ser32), NF-κB p65, phospho-NF-κB p65 (Ser536), and α-tublin (Cell Signaling Technology), followed by incubation with horseradish peroxidase-conjugated goat anti-rabbit IgG or -mouse IgG1 secondary antibody, and detected using a Western blotting detection system (GE Healthcare).

Immunocytochemistry

To visualize p65 nuclear translocation, MSCs were pretreated with parthenolide or vehicle (DMSO) for 6 hours and then cultured with TNF-α (10 ng/mL) for 20 minutes. Cells were fixed with 4% fomaline and permiabilized with Triron-X 100. After washing with PBS, slides were incubated with rabbit anti-p65 antibody (Cell Signaling Technology), followed by incubation with Alexa Fluor 488–conjugated goat anti-rabbit IgG secondary antibody. The actin cytoskeleton was stained with Alexa Fluor 546–conjugated phalloidin (Invitrogen); nuclei were stained with 1,5-bis{[2-(di-methylamino) ethyl]amino}-4,8-dihydroxyanthracene-9,10-dione (DRAQ)-5 dye (Invitrogen). Cells were examined using Keyence BZ-9000.

Results

***In vivo* imaging of MSC accumulation in tumors**

We used bone marrow–derived human MSCs, which expressed characteristic phenotypic markers for MSCs and differentiated into adipocyte, osteocyte, and chondrocyte under specific culture conditions (Supplementary Fig. S1). Then, fiber-modified adenovirus vectors (AdK7) were used for efficient transduction of MSCs and fibroblasts in this study. When the cells were transduced with GFP-expressing AdK7 vectors at a density of 3,000 vp/cell, transduction efficiency was almost 100% (Supplementary Fig. S2A and S2B). The bioluminescent intensity of MSCs transduced with luciferase-expressing Ad vectors at 3,000 vp/cell was equal to that of fibroblasts transduced at 680 vp/cell (Supplementary Fig. S2C). Mice injected with GFP-expressing MSCs or fibroblasts were sacrificed 4 days after injection for immunohistochemical analysis.

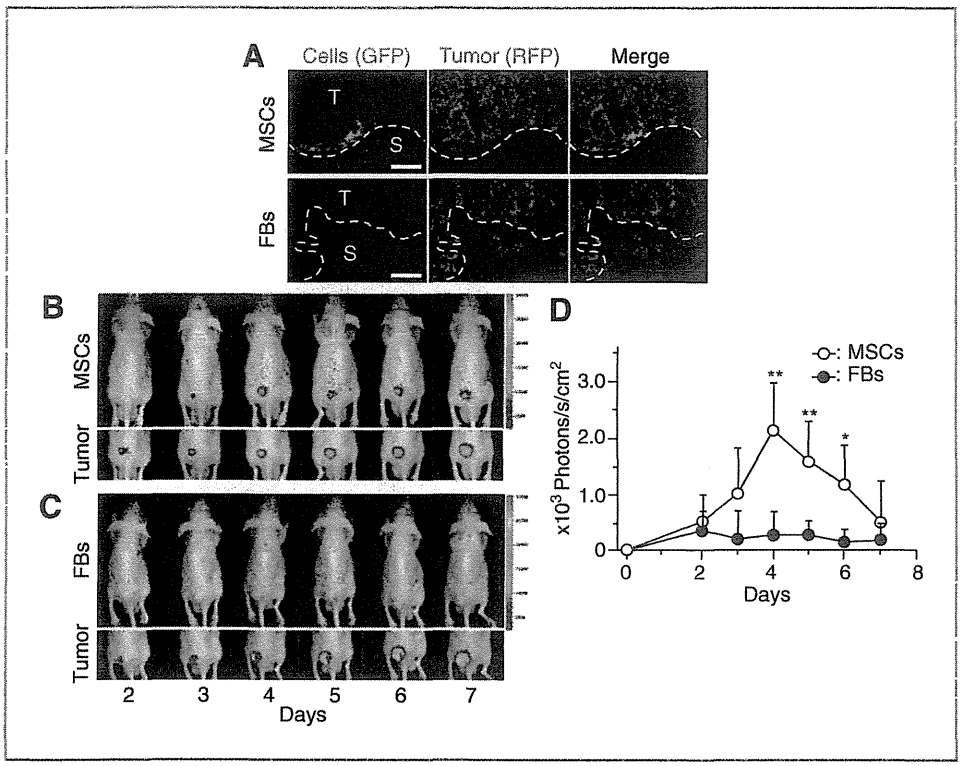

Figure 1. Tumor homing ability of MSCs *in vivo*. A, subcutaneous tumors were induced by injection of SW480/RFP cells (3×10^6) in nude mice (day 0). Cultured MSCs or fibroblasts were transduced with GFP-expressing adenovirus vectors 2 days before injection (day 5) and were injected into the left ventricular cavity (1×10^6, day 7). Mice were sacrificed on day 11, and immunohistochemistry was conducted with anti-GFP antibody on tumor cryosections to detect MSCs or fibroblasts. Top, fluorescent microscopy view of MSC detection; MSCs (left), RFP-labeled tumor cells (center), nucleic staining with DAPI and merge (right). Bottom, fluorescent microscopy view of fibroblast detection; fibroblasts (left), RFP-labeled tumor cells (center), nucleic staining with DAPI and merge (right). Data shown are from 1 representative experiment of 3 carried out. Scale bar, 100 μm. S, stroma; T, tumor. B, luciferase-expressing MSCs were injected into tumor-bearing mice via the left ventricular cavity (1×10^6, day 7). Optical bioluminescence imaging was conducted to periodically trace the cells using IVIS. Top, biodistribution of MSCs as detected by luminescence. Bottom, tumor site detected by red fluorescence. Data shown are from 1 representative experiment of 8 carried out. C, luciferase-expressing fibroblasts were injected into tumor-bearing mice and IVIS imaging was conducted as described earlier. Top, biodistribution of fibroblasts indicated by luminescence. Bottom, tumor site indicated by red fluorescence. Data shown are from 1 representative experiment of 7 carried out. D, bioluminescent intensity at tumor sites was quantified using analysis software. The data are expressed as mean ± SD ($n = 8$ for MSCs and $n = 7$ for fibroblasts). *, $P < 0.05$; **, $P < 0.01$ compared with fibroblasts at the same time.

MSCs identified with anti-GFP antibody were detected in the boundaries of tumors and tumor stroma. However, we found no GFP-positive fibroblasts in the tumor tissues (Fig. 1A). We also used bioluminescence imaging to quantitatively investigate the tumor tropism of MSCs. We injected luciferase-expressing MSCs or fibroblasts into mice through the left ventricular cavity, and then conducted optical bioluminescence imaging to periodically trace the cells using IVIS. In mice injected with luciferase-expressing MSCs, optical bioluminescence at tumor sites became pronounced over time (Fig. 1B), and signal intensity gradually increased (Fig. 1D). In contrast, we observed no signal at the tumor sites in mice injected with luciferase-expressing fibroblasts (Fig. 1C and D).

In vitro migration assays

We analyzed the effects of several growth factors (specifically PDGF-BB, HGF, and VEGF), chemokines (specifically MCP-1 and SDF-1α), and SW480 culture–conditioned medium on MSC and fibroblast migration. These factors are commonly expressed in tumor tissues, and are thought to be potential mediators of MSC tropism. We also used serum-free medium as a negative control and medium containing 30% FBS as a positive control. Migration was quantified by direct labeling and counting of cells by a fluorometer (Fluoroskan Ascent FL; Thermo Labsystems). Exposure to PDGF, HGF, or conditioned medium from SW480 cells stimulated significant MSC migration, whereas VEGF and SDF-1α had no significant effect as compared with serum-free medium (Fig. 2). We compared the migration capacity of MSCs and fibroblasts, the factors that attracted MSCs also induced migration of fibroblasts. Rather, it seems that fibroblasts were more strongly attracted to these factors than MSCs.

In vitro adhesion assays

The tumors generated in mice in this study strongly induced tumor stroma with defined blood vessels, and MSCs specifically accumulated in this stroma (Fig. 3A). Therefore, we propose a hypothesis as follows: factors, as indicated in Fig. 2, attract both MSCs and fibroblasts to the tumor microenvironment, but importantly, MSCs significantly adhere to endothelial cells as

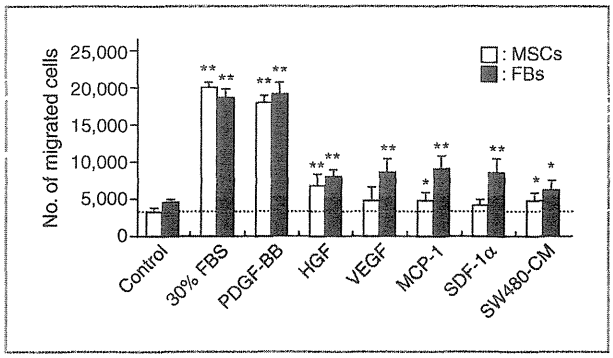

Figure 2. Migratory capacity of MSCs and fibroblasts (FB) in response to growth factors, chemokines, and conditioned medium from SW480 cells. MSCs or fibroblasts were serum-starved for 12 hours. Cells (4×10^4) were added to upper wells of migration chambers. Then, tumor conditioning medium, serum-free medium supplemented with PDGF-BB (10 ng/mL), HGF (30 ng/mL), SDF-1α (150 ng/mL), VEGF-A (25 ng/mL), or MCP-1 (100 ng/mL) were added to the lower wells. Treatment with medium alone (DMEM/F-12) was used as a negative control and treatment with 30% FBS was used as the positive control. The contents of the upper wells and lower wells were separated by polycarbonate filters (8 μm). The data are expressed as mean ± SD ($n = 8$ per cell type). Values are presented as mean ± SE. *, $P < 0.05$ and **, $P < 0.01$ compared with each control.

compared with fibroblasts. Therefore, only MSCs migrate and accumulate at tumor sites via blood vessels in tumor stroma. We speculated that inflammatory cytokines (specifically TNF-α) are required for induction of adhesion molecule expression. First, we measured TNF-α levels in tumor tissues by ELISA. The TNF-α level is significantly higher in tumor tissues as compared with liver and spleen (Fig. 3B). Similar results were also observed in another experiments using Colo205 tumor cells (Supplementary Fig. S3). Then, we assessed the expression of adhesion molecules on endothelial cells, MSCs, and fibroblasts by fluorescence-activated cell sorting analysis. After TNF-α stimulation, endothelial cells and MSCs significantly expressed adhesion molecules including VCAM-1 and VLA-4, compared with fibroblasts (Fig. 3C). We also examined the *in vitro* adhesion of MSCs to endothelial cells. MSCs effectively adhered to endothelial cells as compared with fibroblasts (Fig. 3D). Furthermore, this adhesion was partially inhibited by blocking antibodies against VCAM-1 and VLA-4.

Effects of parthenolide on MSC migration and adhesion

We propose a hypothesis that if TNF-α–induced VCAM-1 expression is inhibited, MSC accumulation at tumors is also attenuated. It is well known that TNF-α induces VCAM-1 expression through the NF-κB signaling pathway. We used parthenolide, a sesquiterpene lactone that occurs naturally in the Feverfew plant. Although parthenolide has several biologic activities, we focused on its suppressive effect on NF-κB activity. At first, there were no differences in migratory capacity toward growth factors or chemokines with or without parthenolide treatment (Fig. 4A). Next, we assessed the inhibitory effect of parthenolide on NF-κB activity: MSCs were pretreated for 6 hours, and then were stimulated with TNF-α for 3 minutes. Parthenolide suppressed p65 nuclear translocation through the inhibition of IκBα phosphorylation (Fig. 4B and C) and strongly inhibited the TNF-α–induced VCAM-1 expression on MSCs (Fig. 4D). Consequently, and MSC–EC adhesion was strongly inhibited by parthenolide treatment similarly to anti-VCAM-1 blocking antibody (Fig. 4E).

In vivo imaging of parthenolide-treated MSCs

First, we examined the effect of parthenolide treatment on transgene expression and cell viability. There were no significant effects on transgene expression and cell viability after parthenolide treatment (Fig. 5A and B). Next, we conducted *in vivo* imaging using IVIS. We observed definite bioluminescence at tumor sites in the mice injected with untreated MSCs (Fig. 5C), and bioluminescent intensity was gradually increased (Fig. 5E), as indicated earlier (Fig. 1B). In contrast, we could not observe definite accumulation at the tumor sites in mice injected with parthenolide-treated MSCs (Fig. 5D and E). Similar results were also obtained by experiments using Colo205 tumor-bearing mice (Supplementary Fig. S4).

Discussion

In this study, we showed that MSC accumulation at tumor sites would be related not only to migratory capacity toward growth factors and chemokines, but also to MSC–EC adhesion following activation by TNF-α. We further showed that NF-κB activity regulates MSC accumulation at tumor sites through the induction of VCAM-1 expression and the resultant interaction with tumor blood vessel endothelial cells.

It is thought that MSCs are mobilized into action following tissue damage, such as injury or inflammation typically accompanied by the release of inflammatory cytokines from the damaged tissues, leading to the recruitment of MSCs to the target. Tumors have a microenvironment consisting of large numbers of inflammatory cells (12). This microenvironment promotes the recruitment of MSCs via various soluble factors secreted by the tumor and inflammatory cells, including EGF, VEGF-A, FGF, PDGF, SDF-1α, IL-8, IL-6, granulocyte colony-stimulating factor (G-CSF), granulocyte-macrophage colony-stimulating factor (GM-CSF), MCP-1, HGF, TGF-β1, and urokinase-type plasminogen activator (uPA; ref. 13). However, in our experimental settings, although systemically injected MSCs accumulated at the tumors, subcutaneously injected MSCs did not (data not shown). We also compared the migration capacity of MSCs and fibroblasts toward growth factors and chemokines *in vitro*. Rather, it seems that fibroblasts were more strongly attracted to these factors than MSCs. Our results suggest that the mechanism of MSC accumulation cannot be explained solely by cytokine-mediated migration. Therefore, we need different viewpoints to clarify the mechanism.

The tumors generated in this study strongly induced tumor stroma with large numbers of blood vessels, and MSCs in particular accumulated in the boundaries between the tumors and tumor stroma. Furthermore, MSC accumulation at the site of the tumors was observed only when cells were injected via the left ventricular cavity. Therefore, we focused on MSC–EC adhesion to elucidate the mechanisms involved.

It has previously been reported that the interaction of MSCs with the vascular endothelium resembles leukocyte chemotaxis (14). To analyze these interactions, we referred to a model

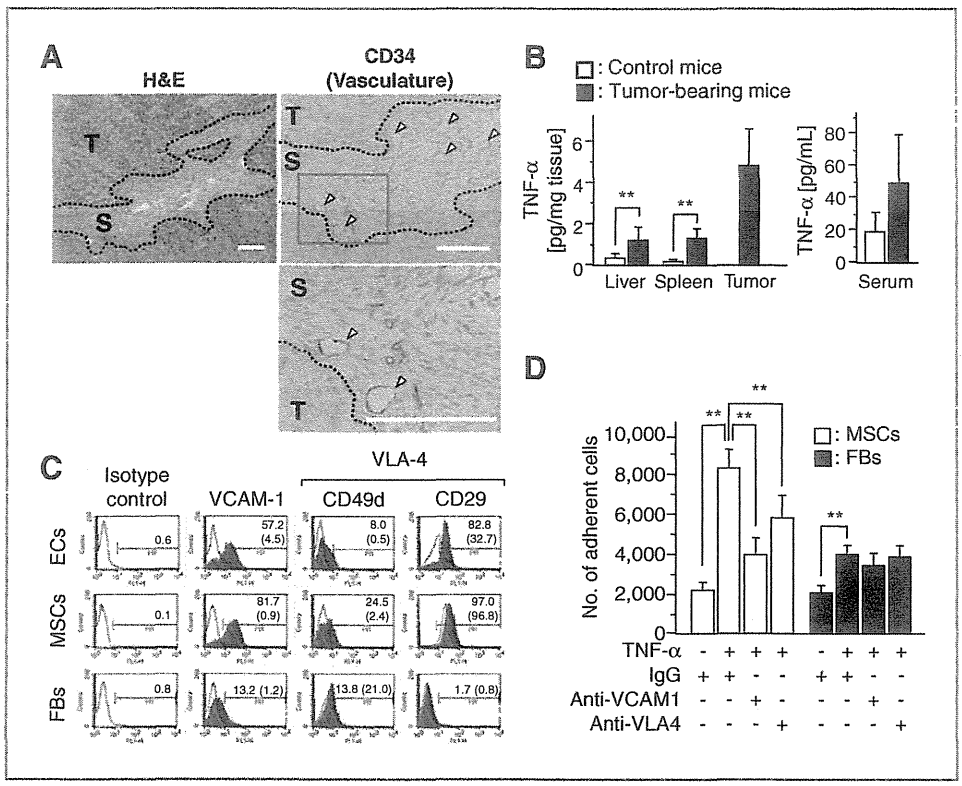

Figure 3. A, sections represent hematoxylin and eosin (H&E) staining (top left), the $CD34^+$ blood vessels/endothelial cells in tumor tissues (top right), the high-power field of view (bottom). Data shown are from 1 representative experiment of 3 carried out. Scale bar, 100 μm. S, stroma; T, tumor. B, specimens of tumor, liver, spleen, and blood were collected from control and tumor-bearing mice. TNF-α levels in tissue homogenates and serum were assayed by ELISA. *, $P < 0.05$; **, $P < 0.01$. C, MSCs, endothelial cells (EC), and fibroblasts were cultured with TNF-α (10 ng/mL) for 6 hours. Cells were labeled with FITC-conjugated antibodies and analyzed by flow cytometry (filled histogram). Rat isotype antibodies IgG1 and IgG2a served as respective controls (open histograms). Values represent the percentage of positive cells after TNF-α stimulation, and values in parentheses represent the percentage of positive cells without TNF-α stimulation. D, endothelial cells were cultured to confluence on fibronectin-coated 96-well plates. Then, MSCs or fibroblasts (1×10^4) were added to cultured endothelial cells. MSCs and endothelial cells were pretreated with the following substances: TNF-α (10 ng/mL), anti-VCAM-1, VLA-4 (10 μg/mL), or isotype control IgG. Values are mean ± SD. **, $P < 0.01$ ($n = 6$ per cell type).

that has been proposed for endothelial cell regulation of leukocyte infiltration in inflammatory tissues. Leukocyte-endothelial adhesion involves dynamic interactions between leukocytes and endothelial cells, and involves multiple steps. These steps must be precisely orchestrated to ensure a rapid response with minimal damage to healthy tissue (15). Interactions between leukocytes and the endothelium are mediated by several families of adhesion molecules, each of which participates in a different phase of the process. The surface expression and activation of these molecules during an inflammatory response is tightly controlled under normal conditions. Inflammatory cytokines including IL-1 and TNF-α involve induction of adhesion molecules. In our experimental settings, although other inflammatory cytokine levels including IL-1 and IL-6 were low (data not shown), significant production of TNF-α was observed. We do not clearly know the source of TNF-α in the tumor at this time, and that our *in vitro* data only suggest that the stroma is the primary source.

As we expected, TNF-α enabled MSCs to adhere to endothelial cells through induction of the expression of adhesion molecules, including VCAM-1 and VLA-4. It is generally considered that VCAM-1 on activated endothelium interacts with the VLA-4 on the leukocyte in the model of leukocyte–endothelial cell adhesion. At first, we speculated that VLA-4 on MSCs plays the same important role as leukocytes. Although both VCAM-1 and VLA-4 on endothelium were efficiently induced by TNF-α stimulation, TNF-α–induced expression of VCAM-1 on MSCs is much stronger than that of VLA-4. Furthermore, MSC–EC adhesion was more effectively inhibited by anti-VCAM-1 antibody as compared with the anti-VLA-4 antibody. On the basis of these results, although VLA-4 on MSC have also related to the MSC-EC adhesion, we thought that VCAM-1 on MSC has more important implications for this adhesion. Once MSCs circulate in the bloodstream, adhesion to endothelial cells is the first step in accumulation in tumors. TNF-α exerts its biologic functions through activating the NF-κB signaling pathway. NF-κB is a major cell survival signal that is antiapoptotic. MSC accumulation was significantly decreased through parthenolide inhibition of NF-κB activity. Although several studies have shown that mitogen-activated protein kinase (MAPK) phosphorylation by growth factors are involved in MSC migration (16, 17), parthenolide did not inhibit MAPK phosphorylation (data not shown). Therefore, at least parthenolide treatment did not affect in migration ability of

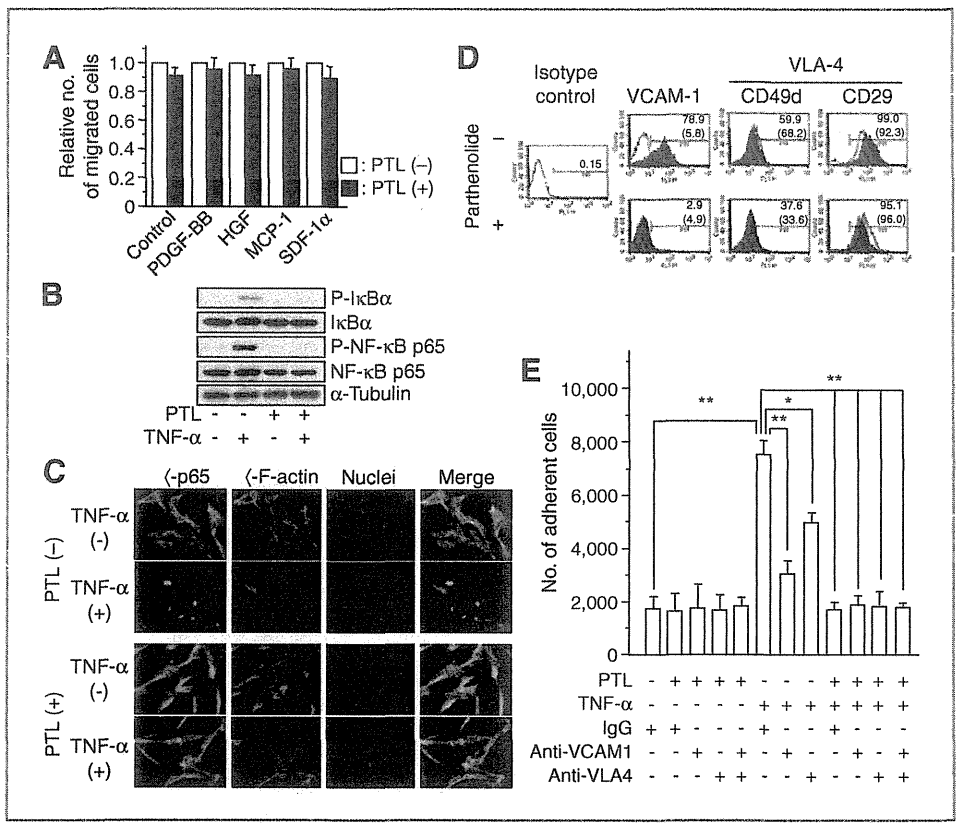

Figure 4. Effect of parthenolide (PTL) on MSC migration and adhesion. A, serum-starved and parthenolide-treated MSCs were added to the upper wells and serum-free medium supplemented with PDGF-BB (10 ng/mL), HGF (30 ng/mL), MCP-1 (100 ng/mL), or SDF-1α (150 ng/mL) was added to the lower wells. Treatment with medium alone (DMEM/F-12) was a negative control and treatment with 30% FBS was the positive control. Values are expressed by relative number of cells compared with respective controls (without pretreatment with parthenolide). B, to assess the inhibitory effect of parthenolide on NF-κB phosphorylation, parthenolide-treated MSCs were stimulated with recombinat TNF-α for 3 minutes, and cellular extracts were prepared for Western blotting. C, to monitor the inhibitory effect of parthenolide on NF-κB activation, immunofluorescent analysis of NF-κB p65 nuclear translocation was conducted as described in Materials and Methods with an Alexa Fluor 488–conjugated specific antibody (green). Actin filaments were labeled with Alexa Fluor 546–conjugated phalloidin (red); nuclei were stained with DRAQ-5 dye (blue). Objective magnification, ×40. D, effect of parthenolide treatment on TNF-α–induced expression of adhesion molecules was analyzed by flow cytometry. Parthenolide-treated MSCs were cultured with TNF-α (10 ng/mL) for 6 hours. Cells were labeled with FITC-conjugated antibodies and analyzed by flow cytometry (filled histogram). Rat isotype antibodies IgG1 and IgG2a served as respective controls (open histograms). Values represent the percentage of positive cells after TNF-α stimulation, and values in parentheses represent the percentage of positive cells without TNF-α stimulation. E, MSCs (1×10^4) were added to endothelial cells that had been cultured to confluence on fibronectin-coated 96-well plates. MSCs and endothelial cells were pretreated with the following substances: parthenolide (5 μmol/L), TNF-α (10 ng/mL), anti-VCAM-1, VLA-4 (10 μg/mL), or isotype control IgG. Values are expressed as mean ± SD ($n = 6$). *, $P < 0.05$ and **, $P < 0.01$.

MSCs toward growth factors from tumors in this experimental settings. Nevertheless, MSC accumulation was significantly decreased through parthenolide inhibition of NF-κB activity. We did not show histologic evidence in the experiments using parthenolide. However, we show that parthenolide does not inhibit luciferase activity *in vitro* (and thus does not seem to be toxic), and that therefore the effect observed *in vivo* should be an effect on recruitment. Although we focused on the function of TNF-α in this study, other inflammatory cytokines including IL-1β and IFN-γ also have ability to induce VCAM-1 expression in target cells (18), and may be involved in MSC accumulation.

TNF-α is a major inflammatory cytokine that plays important roles in diverse cellular events, such as cell survival, proliferation, differentiation, and death. Numerous reports have shown that TNF-α levels in serum are increased in patients with cancer (19, 20), and TNF-α is also related closely to the tumor progression including metastasis. For example, TNF-α intensely induces IL-6 and MCP-1 from cancer-associated fibroblasts and normal fibroblastic cells and has indirect influences on generation of prometastatic microenvironment (21). Furthermore, TNF-α is also released in cardiac infarction, during acute coronary syndromes, and in chronic heart failure; MSCs also accumulate at the site of cardiac infarction (22, 23). These results indicated that proinflammatory cytokines promote homing of stem cells in the heart and that these cytokines have a positive effect on cardiac regeneration. Therefore, activation with TNF-α is one of the critically important steps for MSC accumulation. Moreover, MSC-based tissue-targeted strategies may be adapted for various inflammatory diseases.

In MSC-based cancer-targeted gene therapies, it is thought that therapeutic efficacy is directly linked with accumulation efficiency of MSCs at tumor sites. Our results suggested that combination use of NF-κB inhibitors, including bortezomib, or TNF-α blocking agents, such as infliximab, reduces the

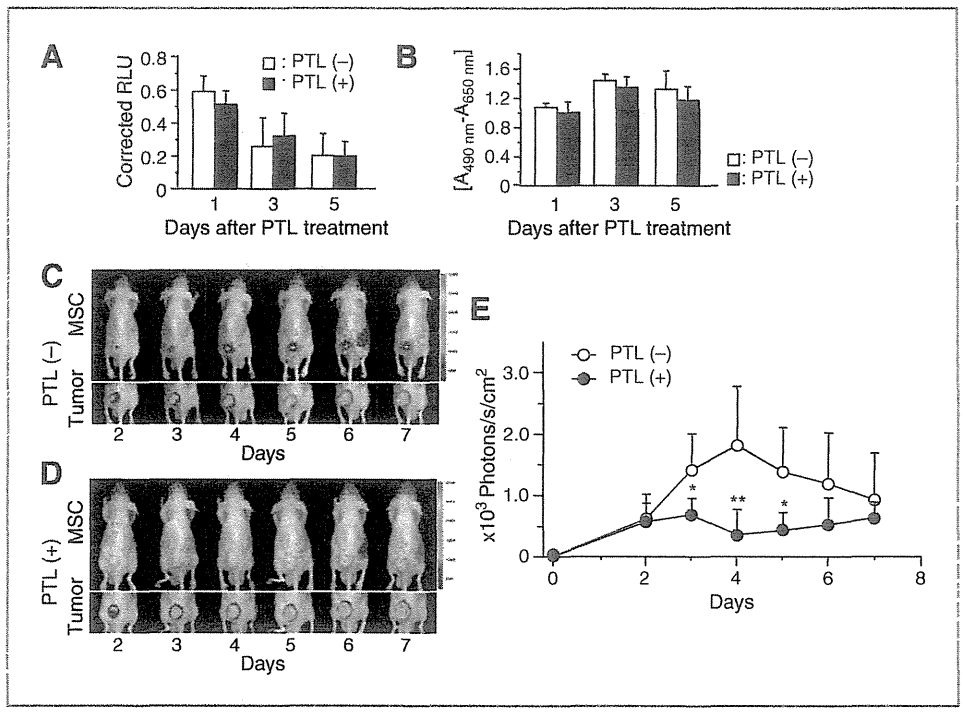

Figure 5. *In vivo* imaging of NF-κB–suppressed MSC accumulation at tumor sites. A, luciferase-expressing MSCs were cultured with parthenolide for 6 hours and luciferase assays were periodically conducted. Values are expressed as mean ± SD ($n = 4$ each). RLU, relative light unit. B, cell viability of parthenolide (PTL)-treated luciferase-expressing MSCs was also examined by XTT assays. Values are expressed as mean ± SD ($n = 4$ each). C, luciferase-expressing MSCs without parthenolide treatment were injected into tumor-bearing mice through the left ventricular cavity and IVIS imaging was periodically conducted. Each data shown are from 1 representative experiment of 8 carried out. D, luciferase-expressing MSCs with parthenolide treatment were injected into tumor-bearing mice and IVIS imaging was periodically conducted. Imaging was conducted as described earlier. Each data shown are from 1 representative experiment of 8 carried out. E, bioluminescent intensity at tumor sites was quantified using analysis software. The data are expressed as mean ± SD ($n = 8$ each). *, $P < 0.05$; **, $P < 0.01$ compared with a group of parthenolide (−) at the same time.

therapeutic efficacy of gene-modified MSCs due to inhibition of the accumulation steps. In contrast, tumor-specific TNF-α–inducing agents would be useful in enhancing therapeutic efficacy, thus further research is required in identifying such agents to more effective therapeutic strategies.

In conclusion, the present study shows that NF-κB activation through TNF-α stimulation and VCAM-1/VLA-4–mediated MSC-EC adhesion may be an important element in MSC accumulation. Although MSCs are useful as cellular vehicles for cancer-targeted gene therapy, past studies have shown that increased MSC accumulation is needed to enhance therapeutic efficacy. Thus, methodology for the enhancement of MSC accumulation should be developed and our findings suggest a solution.

Disclosure of Potential Conflicts of Interest

No potential conflicts of interest were disclosed.

Authors' Contributions

Conception and design: R. Uchibori, H. Mizukami, K. Ozawa
Development of methodology: M. Urabe
Acquisition of data (provided animals, acquired and managed patients, provided facilities, etc.): R. Uchibori
Analysis and interpretation of data (e.g., statistical analysis, biostatistics, computational analysis): R. Uchibori, H. Mizukami, A. Kume
Writing, review, and/or revision of the manuscript: R. Uchibori, M. Urabe, A. Kume
Administrative, technical, or material support (i.e., reporting or organizing data, constructing databases): T. Tsukahara, H. Mizuguchi, Y. Saga, K. Ozawa
Study supervision: M. Urabe, A. Kume, K. Ozawa

Acknowledgments

The authors thank Miyoko Mitsu for her encouragement and technical support.

Grant Support

This work was supported by Grant-in-Aid for Scientific Research (KAKENHI) from the Ministry of Education, Culture, Sports, Science and Technology (21390296 to K. Ozawa), and The Research Award to Jichi Medical School Graduate Student (to R. Uchibori).

The costs of publication of this article were defrayed in part by the payment of page charges. This article must therefore be hereby marked *advertisement* in accordance with 18 U.S.C. Section 1734 solely to indicate this fact.

Received January 13, 2012; revised August 30, 2012; accepted September 11, 2012; published OnlineFirst October 12, 2012.

References

1. Studeny M, Marini FC, Champlin RE, Zompetta C, Fidler IJ, Andreeff M. Bone marrow-derived mesenchymal stem cells as vehicles for interferon-beta delivery into tumors. Cancer Res 2002;62:3603–8.

2. Studeny M, Marini FC, Dembinski JL, Zompetta C, Cabreira-Hansen M, Bekele BN, et al. Mesenchymal stem cells: potential precursors for tumor stroma and targeted-delivery vehicles for anticancer agents. J Natl Cancer Inst 2004;96:1593–603.
3. Nakamizo A, Marini F, Amano T, Khan A, Studeny M, Gumin J, et al. Human bone marrow-derived mesenchymal stem cells in the treatment of gliomas. Cancer Res 2005;65:3307–18.
4. Chen X, Lin X, Zhao J, Shi W, Zhang H, Wang Y, et al. A tumor-selective biotherapy with prolonged impact on established metastases based on cytokine gene-engineered MSCs. Mol Ther 2008;16:749–56.
5. Xin H, Kanehira M, Mizuguchi H, Hayakawa T, Kikuchi T, Nukiwa T, et al. Targeted delivery of CX3CL1 to multiple lung tumors by mesenchymal stem cells. Stem Cells 2007;25:1618–26.
6. Uchibori R, Okada T, Ito T, Urabe M, Mizukami H, Kume A, et al. Retroviral vector-producing mesenchymal stem cells for targeted suicide cancer gene therapy. J Gene Med 2009;11:373–81.
7. Dwyer RM, Potter-Beirne SM, Harrington KA, Lowery AJ, Hennessy E, Murphy JM, et al. Monocyte chemotactic protein-1 secreted by primary breast tumors stimulates migration of mesenchymal stem cells. Clin Cancer Res 2007;13:5020–7.
8. Mizuguchi H, Kay MA. Efficient construction of a recombinant adenovirus vector by an improved *in vitro* ligation method. Hum Gene Ther 1998;9:2577–83.
9. Mizuguchi H, Kay MA. A simple method for constructing E1- and E1/E4-deleted recombinant adenoviral vectors. Hum Gene Ther 1999; 10:2013–7
10. Koizumi N, Mizuguchi H, Utoguchi N, Watanabe Y, Hayakawa T. Generation of fiber-modified adenovirus vectors containing heterologous peptides in both the HI loop and C terminus of the fiber knob. J Gene Med 2003;5:267–76.
11. Mittereder N, March KL, Trapnell BC. Evaluation of the concentration and bioactivity of adenovirus vectors for gene therapy. J Virol 1996;70:7498–509.
12. Coussens LM, Werb Z. Inflammation and cancer. Nature 2002;420: 860–7
13. Honczarenko M, Le Y, Swierkowski M, Ghiran I, Glodek AM, Silberstein LE. Human bone marrow stromal cells express a distinct set of biologically functional chemokine receptors. Stem Cells 2006;24: 1030–41.
14. Rüster B, Göttig S, Ludwig RJ, Bistrian R, Müller S, Seifried E, et al. Mesenchymal stem cells display coordinated rolling and adhesion behavior on endothelial cells. Blood 2006;108:3938–44.
15. Butcher EC. Leukocyte-endothelial cell recognition: three (or more) steps to specificity and diversity. Cell 1991;67:1033–6.
16. Coffelt SB, Marini FC, Watson K, Zwezdaryk KJ, Dembinski JL, LaMarcad HL, et al. The pro-inflammatory peptide LL-37 promotes ovarian tumor progression through recruitment of multipotent mesenchymal stromal cells. Proc Natl Acad Sci U S A 2009; 106:3806–11.
17. Zhang A, Wang Y, Ye Z, Xie H, Zhou L, Zheng S. Mechanism of TNF-α-induced migration and hepatocyte growth factor production in human mesenchymal stem cells. J Cell Biochem 2010;111: 469–75.
18. Hosokawa Y, Hosokawa I, Ozaki K, Nakae H, Matsuo T. Cytokines differentially regulate ICAM-1 and VCAM-1 expression on human gingival fibroblasts. Clin Exp Immunol 2006;144:494–502.
19. Ferrajoli A, Keating MJ, Manshouri T, Giles FJ, Dey A, Estrov Z, et al. The clinical significance of tumor necrosis factor-alpha plasma level in patients having chronic lymphocytic leukemia. Blood 2002;100: 1215–9.
20. Ahmed MI, Salahy EE, Fayed ST, El-Hefnawy NG, Khalifa A. Human papillomavirus infection among Egyptian females with cervical carcinoma: relationship to spontaneous apoptosis and TNF-alpha. Clin Biochem 2001;34:491–8.
21. Mueller L, von Seggern L, Schumacher J, Goumas F, Wilms C, Braun F, et al. TNF-alpha similarly induces IL-6 and MCP-1 in fibroblasts from colorectal liver metastases and normal liver fibroblasts. Biochem Biophys Res Commun 2010;397:586–91.
22. Shake JG, Gruber PJ, Baumgartner WA, Senechal G, Meyers J, Redmond JM, et al. Mesenchymal stem cell implantation in a swine myocardial infarct model: engraftment and functional effects. Ann Thorac Surg 2002;73:1919–25.
23. Pittenger MF, Martin BJ. Mesenchymal stem cells and their potential as cardiac therapeutics. Circ Res 2004;95:9–20.

Gene Therapy (2012) 19, 476–482

www.nature.com/gt

ORIGINAL ARTICLE

Interleukin-10 expression induced by adeno-associated virus vector suppresses proteinuria in Zucker obese rats

M Ogura[1,2], M Urabe[1], T Akimoto[2], A Onishi[1,2], C Ito[2], T Ito[3], T Tsukahara[1], H Mizukami[1], A Kume[1], S Muto[2], E Kusano[2] and K Ozawa[1]

Varying degrees of metabolic abnormalities mediated by chronic inflammation are implicated in the chronic glomerular injuries associated with obesity. Interleukin (IL)-10, a pleiotropic cytokine, exerts anti-inflammatory effects in numerous biological settings. In the present study, we explored the biological benefits of adeno-associated virus (AAV) vector-mediated sustained IL-10 expression against the pathological renal characteristics observed in Zucker fatty rats (ZFRs). We injected an AAV vector, encoding rat IL-10 or enhanced green fluorescent protein (GFP) into male ZFRs at 5 weeks of age. Subsequently, the renal pathophysiological changes were analyzed. Persistent IL-10 expression significantly reduced the urinary protein excretion of ZFRs compared with GFP expression (47.1 ± 11.6 mg per mg·creatinine versus 88.8 ± 30.0 mg per mg·creatinine, $P<0.01$). The serum levels of IL-10 negatively correlated with the urinary protein in AAV-treated rats ($r=-0.78$, $P<0.01$). Renal hypertrophy, increased widths in the glomerular basement membrane, and the lack of uniformity and regularity of the foot process of the visceral glomerular epithelial cells of ZFRs were significantly blunted by IL-10 expression. IL-10 also abrogated the downregulation of glomerular nephrin observed in ZFRs treated with the GFP vector. Our findings provide insights into the potential benefit of the anti-inflammatory effects of IL-10 on the overall management of glomerulopathy induced by the metabolic disorders associated with obesity.
Gene Therapy (2012) **19**, 476–482; doi:10.1038/gt.2011.183; published online 24 November 2011

Keywords: obesity; nephrin; glomerular hyperfiltration; glomerular epithelial cells; glucose intolerance

INTRODUCTION

Numerous pathophysiological disorders have been demonstrated to be related to obesity.[1] Not exceptionally, accumulating evidence also suggests a role for obesity in the development of chronic kidney disease.[2–4] The renal effects of obesity in humans and experimental animals include both functional and morphological adaptations, such as an increased glomerular filtration rate, increased renal blood flow, and renal hypertrophy with focal segmental glomerulosclerosis.[5–7] Although the qualitative and quantitative information about the pathogenesis of the glomerulopathy associated with obesity remains to be delineated, varying degrees of metabolic abnormalities appear to be involved. Indeed, hyperinsulinemia resulted in the stimulation of the synthesis of insulin-like growth factors, and the upregulation of transforming growth factor-β1 by elevated serum leptin has been implicated in the chronic glomerulopathy associated with obesity.[8,9] Moreover, hyperlipidemia may also promote glomerulosclerosis through mechanisms in which engagement of lipoprotein receptors on mesangial cells, oxidative cellular injury, macrophage chemotaxis and accelerated synthesis of fibrogenic cytokines are involved.[10]

Interleukin (IL)-10 is a multifunctional cytokine with anti-inflammatory properties.[11] Accumulating evidence suggests potential roles for IL-10 in the management of several pathophysiological disorders, including obesity. Indeed, IL-10 has been shown to not only reduce cholesterol levels, but also to improve the insulin resistance in experimental animal models.[12,13] Moreover, it has also been reported that obese patients and subjects with metabolic syndrome have a lower level of serum IL-10 than healthy normal subjects.[14] These observations led us to consider the therapeutic potential of modulating inflammation by IL-10 in the overall management of obese patients.

In the present study, we evaluated the effects of IL-10 on the renal characteristics of Zucker fatty (Zucker-fa/fa) rats, which have recently been focused on as an experimental animal model of renal injuries mediated by obesity-associated metabolic disorders.[7,15,16] The biological efficiency of the systemic administration of recombinant IL-10 seems to be insufficient because of the immediate decrease resulting from its short bioactive half-life.[17] Instead, we have transferred the gene encoding IL-10 using an adeno-associated virus (AAV) vector, as these vectors can be used to transduce skeletal muscle, thereby inducing the systemic and sustained expression of potentially therapeutic proteins following a single intramuscular administration.[12,18]

RESULTS

The expression of IL-10 in Zucker rats

Our first series of experiments verified the integrity of our vectors in the Zucker-fa/fa rats. The serum concentrations of IL-10 in the rats were determined at 5, 10, 15, 20 and 25 weeks after the initial treatments, which included the administration of phosphate buffer saline (PBS) and transductions of the recombinant AAV type 1-based vector carrying the rat IL-10 (AAV–IL-10) or control-enhanced green fluorescent protein gene (AAV–GFP). As shown in Figure 1,

[1]Division of Genetic Therapeutics, Center for Molecular Medicine, Jichi Medical University, Shimotsuke, Japan; [2]Division of Nephrology, Department of Medicine, Jichi Medical University, Shimotsuke, Japan and [3]Division of Cardiovascular Medicine, Department of Medicine, Jichi Medical University, Shimotsuke, Japan
Correspondence: Dr M Ogura, Division of Nephrology, Department of Internal Medicine, Jichi Medical School, 3311-1 Yakushiji, Shimotsuke-Shi, Tochigi 329-0498, Japan.
E-mail: m-ogura@jichi.ac.jp
Received 25 May 2011; revised 21 September 2011; accepted 17 October 2011; published online 24 November 2011

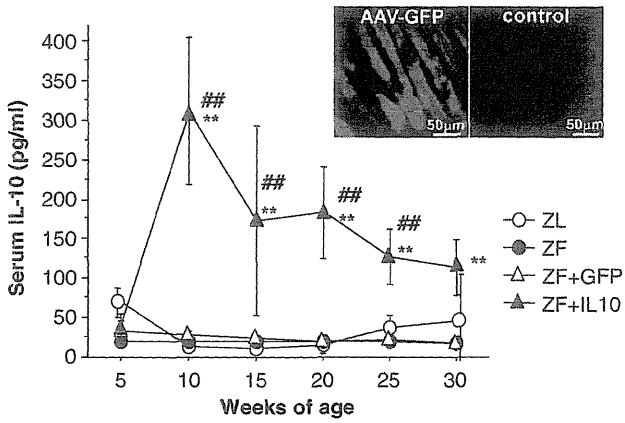

Figure 1 The longitudinal changes in serum concentrations of IL-10 at 5, 10, 15, 20 and 25 weeks after the initial sham treatments (PBS alone), and transductions of AAV–IL-10 or AAV–GFP into the Zucker fa/fa rats or lean littermates. Inset: an analysis of the cryostat sections of the anterior tibial muscles injected with AAV–GFP or PBS (control). The immunofluorescence analyses performed 10 weeks post-vector injections revealed ubiquitous GFP expression within the muscle tissue, thus suggesting efficient gene transduction by the AAV vectors. Scale bar is indicated in each panel. The data are the means ± s.d. (n=6). $^{**}P<0.01$ versus ZF and ZF+GFP groups; $^{\#\#}P<0.01$ versus the value at 5 weeks of age.

statistically significant increases in serum IL-10 were confirmed in Zucker-fa/fa rats administered AAV–IL-10 (sham Zucker-fa/fa rats administered PBS (ZF)+IL-10), whereas the levels in Zucker-fa/fa rats administered AAV–GFP (ZF+GFP), ZF and control Zucker lean littermates (Zucker +/+) administered PBS (ZL) were comparable. The levels of IL-10 in ZF+IL-10 were about 12-fold higher at week 5, and an average of 5-fold higher than ZF, ZF+GFP and ZL groups at 25 weeks after the initial treatments.

The effects of IL-10 on clinical and laboratory characteristics

The body weights of all rats were increased during the observation period. Although the degree of the increases was significantly higher in the Zucker-fa/fa rats than in the ZL rats, the mean body weights of ZF, ZF+GFP and ZF+IL-10 at each time point were comparable (Figure 2a). Similarly, the food consumption of the Zucker-fa/fa rats was significantly greater than that of the ZL, although there were no significant differences in the amount of food intake in the three Zucker-fa/fa rat groups (Figure 2b). On the other hand, the serum levels of total cholesterol (Tcho) and triglycerides (TG) were significantly higher in Zucker-fa/fa rats compared with ZL throughout the observation period. However, in the ZF+IL-10, the serum Tcho was significantly lower than those in the ZF and ZF+GFP (Figure 2c). Similar trends were also confirmed in the longitudinal changes in the serum TG. As shown in Figure 2d, Zucker-fa/fa rats had significantly higher serum TG than their lean littermates; however, the expression of IL-10 seemed to negatively affect the level of TG. At 30 weeks of age, these parameters negatively correlated with the IL-10 level in the Zucker-fa/fa rats with PBS or AAV treatment (Figures 2e and f). During the observation period, no significant difference in the systolic blood pressure was observed in the Zucker-fa/fa rats treated with PBS or the AAV, although there was a trend for the systolic blood pressure in the ZL to be higher than that of all of the Zucker-fa/fa rats (data not shown).

We next analyzed the effect of IL-10 on the parameters related to the glucose metabolism. As shown in Table 1, the fasting blood glucose levels of Zucker-fa/fa rats were significantly higher at 10 weeks after the administration of the vector with GFP or PBS administration compared with the lean littermates. At 30 weeks of age, we determined the blood hemoglobin A1c (HbA1c) and serum immuno-reactive insulin levels. As shown in Figure 3a, the transduction of IL-10 reversed the increase in the levels of HbA1c that was confirmed in ZF and ZF+GFP rats, thus suggesting that IL-10 might have a role in improving the disturbance of the fed-state glucose metabolism in the Zucker fa/fa rats. Indeed, the fed state serum insulin level was significantly elevated in ZF+IL-10 rats compared with the other groups, whereas the levels of fasting serum insulin in the Zucker-fa/fa rats were comparable (Figure 3b).

The effects of IL-10 on renal characteristics

We also explored the effects of IL-10 on the renal characteristics of the obese rats. As shown in Figure 4a, all three groups of obese rats (ZF, ZF+GFP and ZF+IL-10) demonstrated a gradual increase in urinary protein in a time-dependent manner, and the urinary protein level in the ZF and ZF+GFP finally increased up to 102.2 ± 21.9 and 88.8 ± 30.0 mg per mg·creatinine, respectively. At 30 weeks of age, the urinary protein in the ZF+IL-10 (47.1 ± 11.6 mg per mg·creatinine) was significantly lower than in the other Zucker-fa/fa rats groups ($P<0.01$). Moreover, the serum levels of IL-10 negatively correlated with the urinary protein level in Zucker-fa/fa rats ($r=-0.88$, $P<0.01$, $n=17$; Figure 4b). During the observation period, the creatinine clearance (Ccr) in obese rats without IL-10 was significantly increased at both 25 and 30 weeks of age (Figure 4c). There was also a negative correlation between the serum IL-10 level and Ccr ($r=-0.65$, $P<0.01$, $n=15$; Figure 4d).

Figure 5 shows the anatomical and morphological effects of IL-10 on the Zucker-fa/fa rats. All three groups of Zucker-fa/fa rats had significantly higher kidney weights than the ZL at 30 weeks of age. However, the expression of IL-10 caused a significant decrease in the kidney weight when compared with the ZF and ZF+GFP (1.70 ± 0.13 g versus 1.86 ± 0.12 g, $P<0.05$, and 1.85 ± 0.09 g, $P<0.05$, respectively; Figure 5a). When viewed under a light microscope, there were no apparent histological changes compatible with glomerulosclerosis and cellular infiltrations within the glomerulus in any of the subjects; however, the Zucker-fa/fa rats had a larger area of glomeruli than the ZL, which was significantly reduced by the persistent expression of IL-10 in the ZF+IL-10 (Figures 5b and c). Transmission electron microscopy showed the hyperplastic glomerular basement membrane (GBM) and prominent foot process effacement in ZF and ZF+GFP (Figure 5b), but these changes seemed to be prevented or reversed in the ZF+IL-10. Indeed, there were significant differences in the mean width of the GBM between the ZF+IL-10 and the other two groups of Zucker-fa/fa rats (Figure 5d). The lack of uniformity and regularity of the foot process demonstrated by scanning electron microscopic was remarkable in the ZF and ZF+GFP, but this was not observed in the ZF+IL-10 and ZL (Figure 5b).

The effects of IL-10 on the expression of nephrin within the glomeruli of Zucker-fa/fa rats

To determine the potential mechanisms of the counter-effect of IL-10 on the changes in the renal characteristics in the Zucker-fa/fa rats, we evaluated the effects of IL-10 on the expression of nephrin within glomeruli. As shown in Figure 6, the glomerular nephrin expressions in Zucker fa/fa rats treated with PBS or AAV–GFP were significantly diminished compared with that of lean littermates, and the transduction of IL-10 apparently reversed the reduced expression of nephrin within glomeruli that was observed in the Zucker-fa/fa rats (Figure 6).

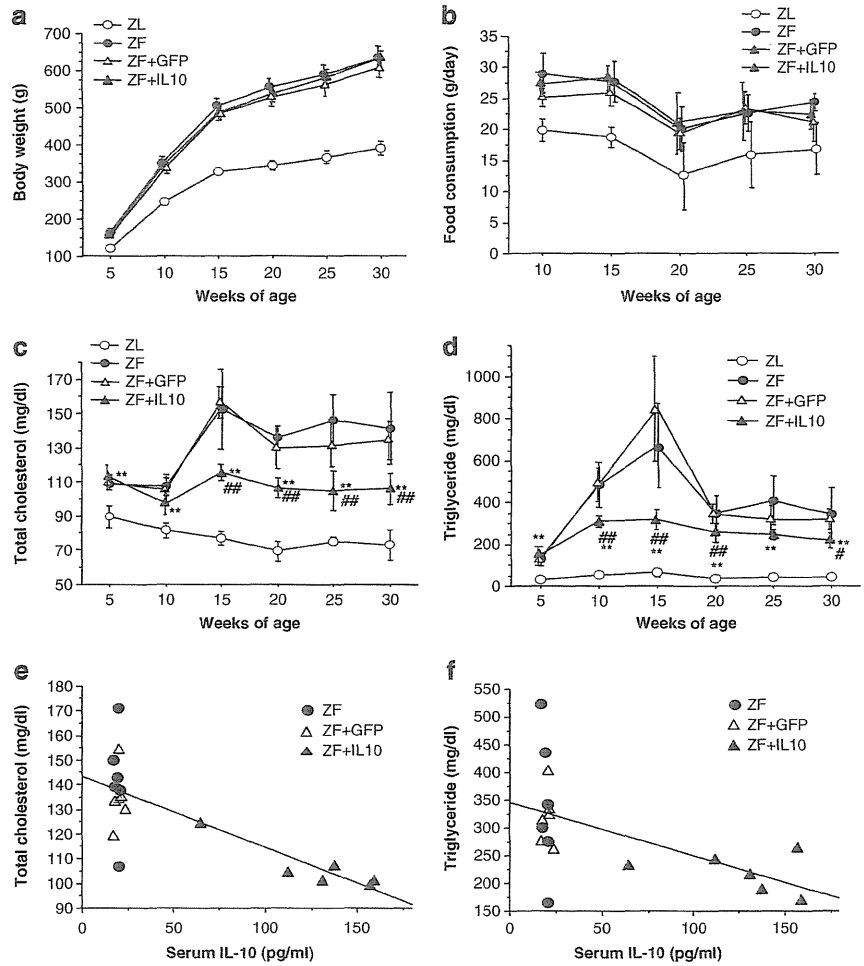

Figure 2 The changes in the body weights (**a**), food consumption (**b**), serum Tcho (**c**) and serum TG (**d**). The body weights and food consumption were significantly higher in obese rats than in lean littermates at each point time. Note that the body weights and the food consumption in the three groups of obese rats were comparable, whereas the serum Tcho and TG levels were significantly lower than those in the ZF and ZF+GFP groups. The data are the means ± s.d. (n=6). $^{**}P<0.01$ versus the control; $^{\#}P<0.05$, $^{\#\#}P<0.01$ versus ZF and ZF+GFP groups. The relationships between IL-10 and Tcho (**e**) and TG (**f**) were also evaluated (groups: ZF, ZF+GFP and ZF+IL-10; n=6 per group; $r=-0.77$, $P<0.01$ and $r=-0.77$, $P<0.01$, respectively).

Table 1 Changes in FBS in Zucker fa/fa rats and age-matched control lean littermates

Age (weeks)	*ZL*	*ZF*	*ZF+GFP*	*ZF+IL-10*
10	127.2 ± 12.1	157.5 ± 21.0[a]	175.5 ± 19.6[a]	175.8 ± 24.5[a]
20	120.2 ± 7.3	126.3 ± 13.5	129.2 ± 11.5	139.2 ± 22.1[a]
30	108.8 ± 14.3	118.7 ± 16.3	135.3 ± 20.0[a]	126.8 ± 10.8[a]

Abbreviations: FBS, fasting blood glucose; GFP, green fluorescent protein; IL, interleukin; ZF, sham Zucker-fa/fa rats administered PBS; ZL, Zucker lean littermates (Zucker +/+) administered PBS. [a]$P<0.05$ versus ZL.

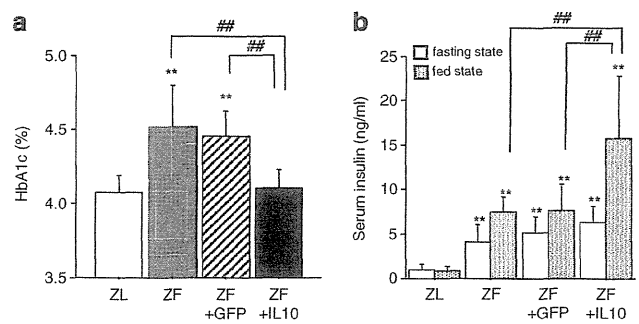

Figure 3 The effect of the IL-10 expression on the level of blood HbA1c (**a**) and serum immunoreactive insulin (**b**). The data were determined with blood samples obtained from rats at 30 weeks of age. $^{**}P<0.01$ versus the control and $^{\#\#}P<0.01$, respectively.

DISCUSSION

The present study clearly demonstrates for the first time that IL-10, delivered by an AAV vector, suppresses the changes in renal characteristics in obese rats, including the increase in urinary protein, elevated Ccr, glomerular hypertrophy and the decreased glomerular expression of nephrin, without affecting the body weight and food intake of the rats. These results suggest the potential benefits of IL-10 in the management of obese subjects with renal pathophysiological abnormalities.

Numerous studies have focused on the abnormalities in lipid metabolism as a potential mechanism underlying various types of glomerular injuries, and the treatment of hyperlipidemia has been shown to reduce the excretion of urinary proteins and to decrease the

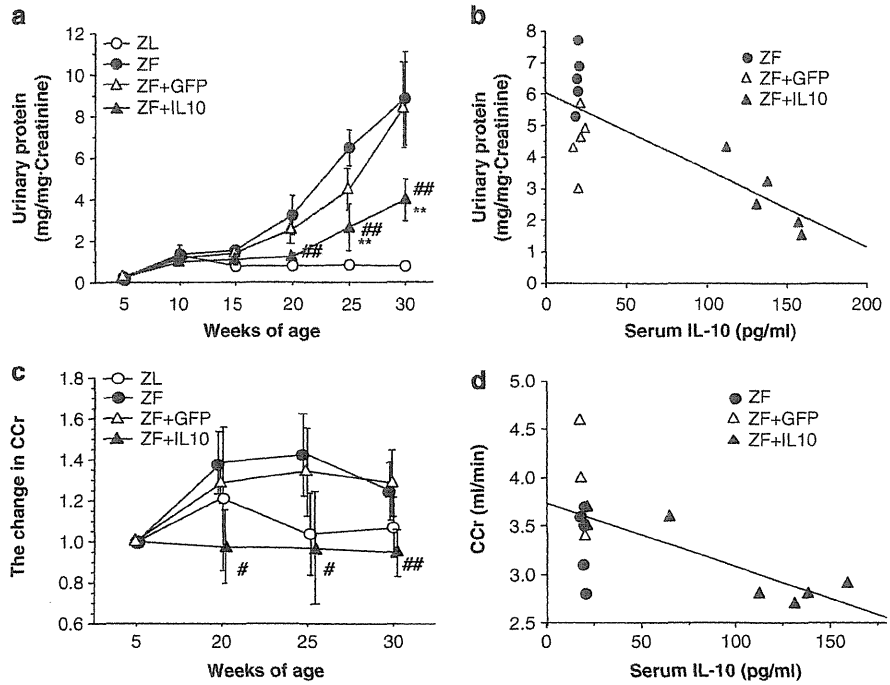

Figure 4 The effects of the IL-10 expression on urinary protein excretion (**a**) and the changes in the Ccr (**c**) in the ZF (●), ZF+GFP (▲), ZF+IL-10 (▲) and ZL (○) rats. The data are the means ± s.d. (n=5–6). $^{**}P<0.01$ versus the controls; $^{\#}P<0.05$, $^{\#\#}P<0.01$ versus ZF or ZF+GFP groups. The relationship between IL-10 and the urinary protein excretion (**b**) or the change in the Ccr (**d**) in the obese rats (groups: ZF, ZF+GFP or ZF+IL-10; n=5–6 per group; r=−0.78, $P<0.01$ and r=−0.65, $P<0.01$, respectively).

glomerular injury characterized by mesangial matrix expansion and focal segmental glomerulosclerosis, which are typical of Zucker fa/fa rats at about 60 weeks of age, without any changes in glomerular hemodynamic function.[7,10,16,19] As such renal structural alterations seem to be relatively nonspecific and may represent part of a common final pathway,[15] we focused on the changes in renal characteristics that precede the development of mesangial matrix expansion and focal segmental glomerulosclerosis. Consistently, the histological analyses of our Zucker fa/fa rats performed at 30 weeks of age failed to demonstrate such glomerular lesions. Instead, glomerular hypertrophy, an increase in the widths of the GBM and the elevation of Ccr due to presumable glomerular hyperfiltration, which have all been implicated in hyperglycemia and are considered to be early events followed by diabetic glomerulosclerosis among diabetic subjects,[20–22] were observed.

These findings might not be surprising, as abnormal glucose metabolism characterized by mild hyperglycemia, as well as hyperinsulinemia and insulin resistance, are alternative metabolic characteristics of Zucker fa/fa rats.[7,15,23] Obviously, this was also the case with the present study. Of note, IL-10 seems to improve the disturbed fed-state glucose metabolism of the Zucker fa/fa rats, as the HbA1c in ZF-IL-10 rats was significantly decreased compared with the rest of the obese groups. The recovery from advanced insulin resistance is unlikely to be implicated in these rats. Instead, the accelerated increase in serum insulin seems to be involved in the countervailing effect of IL-10 on the glucose intolerance. Such an increase in serum insulin may be attributable to a change in the metabolic clearance or altered sensitivity to blood glucose. Alternatively, IL-10 might stimulate pancreatic β-cell function.[24] Although the elevation of serum insulin seemed to be necessary for glycemic control among our obese animals, one may argue that this might have adverse consequences on the renal tissue, and thus, might contribute to the development of a wide range of glomerular and interstitial injuries associated with disturbed glucose metabolism.

Indeed, it has been shown that hyperinsulinemia pleiotropically affects the kidney tissue through various pathways.[8,9,25] Nevertheless, renal pathophysiological evaluations failed to confirm the adverse effect of hyperinsulinemia in ZF-IL10 rats. Our results suggest that the biological significance of the improvement in glucose intolerance, mediated by the further increase in serum insulin induced by IL-10, on the renal characteristics of Zucker fa/fa rats should exceed that of hyperinsulinemia. Otherwise, an alternative process independent of the regulation of obesity-related metabolic disturbance might be involved in the countervailing effect of IL-10 on the renal pathophysiological characteristics among our obese animals.

Whether the glomerular morphological changes demonstrated in the present study cause or contribute to the presumable development of mesangial matrix expansion and focal segmental glomerulosclerosis in Zucker-fa/fa rats, which have been demonstrated to have abnormal lipid metabolism at ages older than 30 weeks,[7,10,16,19] remains to be determined. However, the fact that there were significant decreases in the serum levels of Tcho and TG in the ZF+IL-10 rats led us to consider that the early phase of the changes in the renal characteristics of Zucker fa/fa rats might be modulated, at least in part, by IL-10 through the reduction of Tcho and TG. Although the course of the etiological linkage between IL-10 and TG remains to be delineated, previous data suggest that IL-10 might have a direct effect on the cholesterol metabolism through the suppression of the hydroxymethylglutaryl-CoA reductase expression, thereby lowering the Tcho level.[12]

A hyperplastic GBM is often accompanied by changes in the visceral glomerular epithelial cells, that is, podocytes, and a progressive loss of podocyte foot processes associates with narrowing of the filtration slits, whereas the number of podocytes decreases with the increase in

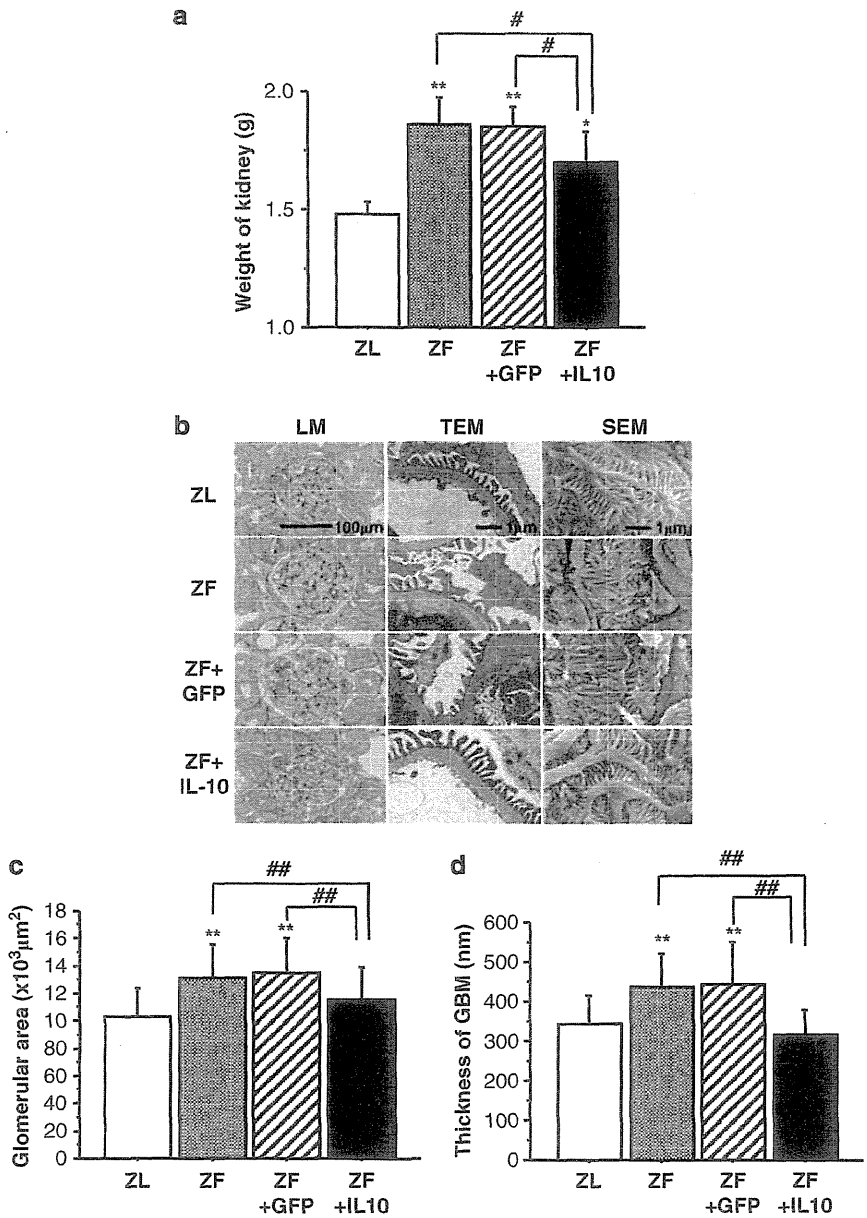

Figure 5 The effects of IL-10 expression on the renal morphological changes in ZFRs. (**a**) The changes in the weights of the kidneys of ZF (black hatched box), ZF+GFP (black striped box), ZF+IL-10 (black box) and ZL (white box) rats. The results were presented as means ± s.d. (n=5). *P<0.05, **P<0.01, versus the controls; $^{\#}P$<0.05 versus the ZF and ZF+GFP groups. (**b**) Representative photomicrographs of periodic acid-Schiff-stained light microscopic, transmission electron microscopy and scanning electron microscopic views. The scale bars are shown in the panel for the control lean littermates. (**c**) The differences in the glomerular area of the ZF (black hatched box), ZFtGFP (black striped box), ZFtIL-10 (black box) and ZL (white box) rats. (**d**) The differences in the width of the GBM of ZF (black hatched box), ZFtGFP (black striped box), ZFtIL-10 (black box) and ZL (white box) rats. The results are presented as the means ± s.d. **P<0.01 versus the controls; $^{\#\#}P$<0.01 versus the ZF and ZF ± GFP groups.

urinary protein excretion.[26,27] Although the precise number of podocytes was not quantified in the present study, such pathogenic processes were likely modulated by IL-10, as the prominent foot process effacement associated with the hyperplastic GBM, and the lack of uniformity and regularity of the foot process confirmed in ZF and ZF-GFP were recovered in ZF+IL-10. Moreover, IL-10 remarkably blunted the reduced glomerular expression of nephrin, which has been located to the slit diaphragm of glomerular podocytes, where it acts as a renal ultrafilter barrier function.[28] Although the mechanism leading to the downregulation of glomerular nephrin in our rats is not well characterized, the potential role of reactive oxygen species, and particularly, the balance of lipid peroxidase, was recently proposed to account for the decrease in nephrin mRNA in experimental glomerulopathy.[29] Therefore, it is reasonable to consider that IL-10 should directly or indirectly modulate such pathophysiological processes within our obese subjects.

Although the present study provides information regarding the effects of IL-10 on the renal characteristics of the Zucker fa/fa rats, our results should be interpreted within the context of the study's limitations. First, the number of animals included in each group was small, implying that the study may be underpowered for the evaluation of several parameters, and selection bias may also be present. Indeed, our

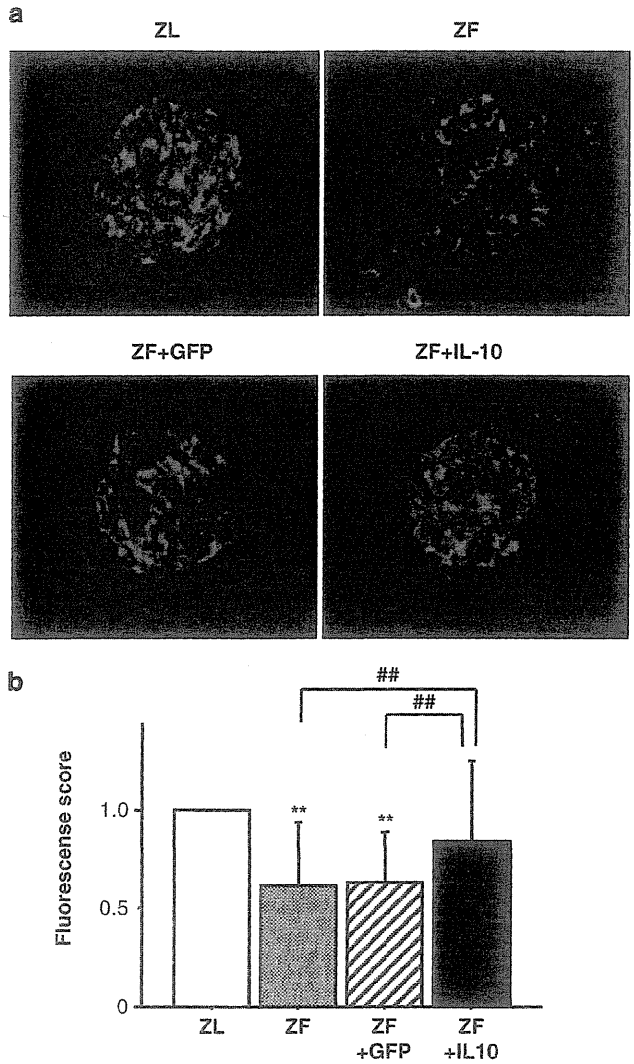

Figure 6 Immunofluorescent staining of glomerular nephrin from ZFRs and control littermates. (**a**) Representative microscopic views are shown. (**b**) The fluorescence intensity of each view was also quantified using arbitrary units. $^{**}P<0.01$ versus control littermates; $n=6$; $^{\#\#}P<0.01$ versus the ZF and ZF+GFP groups.

findings, demonstrating that the mean body weights and the food consumption levels of each of the obese groups, might have been underestimated, as it has been reported that IL-10 could attenuate the changes in food intake and energy expenditure in the experimental rat model of acute inflammatory disturbance associated with bacterial infection.[30] It may be interesting to determine whether the IL-10 treatment applied to our obese rats affected their glucose and lipid metabolism without inducing any change in their body weight and food consumption. Whether our findings remain true when the number of subjects is increased should be evaluated in greater detail in a future study.

In summary, AAV vector-mediated IL-10 gene transfer into the Zucker fa/fa rats could introduce efficient and stable IL-10 expression, resulting in the marked reduction of urinary protein excretion. These changes were associated with the recovery of renal structural alterations. Our observations indicate the presence of complex interactions between the changes in the renal characteristics of Zucker fa/fa rats and the inflammatory cascade, as well as the potential benefit of the anti-inflammatory effects of IL-10 in the overall management of glomerulopathy mediated by obesity-related metabolic disorders.

METHODS

AAV vector production

DNA encoding rat IL-10 was PCR-amplified from rat splenocyte complementary DNA as described previously, using the primers 5′-GCACGAGAGCCAC AACGCa-3′ and 5′-GATTTGAGTACGATCCATTTATTCAAAACGAGGAT-3′.[18] For efficient transgene expression in the skeletal muscle, we constructed a recombinant AAV type 1 vector, which carried the *IL-10* gene or *GFP* gene, controlled by the modified chicken β-actin promoter with the cytomegalovirus posttranscriptional regulatory element (a generous gift from Dr Thomas Hope, Infectious Disease Laboratory, Salk Institute). AAV vectors were prepared according to the previously described three-plasmid transfection adenovirus-free protocol, with minor modification to use the active gassing system.[18,31] Briefly, 60% confluent human embryonic kidney 293 cells incubated in a large culture vessels were co-transfected with the proviral transgene plasmid, AAV-1 chimeric helper plasmid (p1RepCap), and the adenoviral helper plasmid pAdeno (Avigen Inc., Alameda, CA, USA).[31] The crude viral lysates were purified by two rounds of CsCl in a two-tier centrifugation. The titer of the viral stock was determined against plasmid standards by using dot blot hybridization, after which the stock was diluted in PBS before injection.

Animal model and experimental design

All animal procedures were approved by the Jichi Medical University ethics committee and were performed in accordance with the National Institutes of Health Guide for the Care and Use of Laboratory Animals. Male Zucker-fa/fa and Zucker +/+ rats were obtained from Japan SLC Inc (Shizuoka, Japan). Animals were housed in a temperature and humidity controlled room, and standard rat chow (CE-2, Clea Japan, Inc., Tokyo, Japan) and water were available *ad libitum*. Five-week-old male Zucker-fa/fa rats were randomly divided into three groups ($n=6$ in each group): that is, ZF, ZF+GFP and ZF+IL-10. Control lean littermates administered PBS (ZL) were also included in the study. Under ether anesthesia, the PBS buffer or AAV vectors in PBS were injected into the bilateral anterior tibial muscles of the rats (200 μl per site, 1×10^{11} genome copies per rat). For each animal, body weight and food consumption were measured at 5, 10, 15, 20, 25 and 30 weeks of age. Urinary samples were collected in metabolic sampling bottles over 24 h. Blood samples were collected by tail clipping under ether anesthesia after the rats had fasted for 16 h. In some circumstances, morning blood samples were also collected to determine the fed-state blood glucose and serum immunoreactive insulin levels. The serum levels of Tcho (Cholesterol C-test; Wako Chemicals, Tokyo, Japan), TG (L-Type TG H Kit; Wako Chemicals) and IL-10 (Quantikine ELISA Kit; R&D systems, Minneapolis, MN, USA) were determined according to the manufacturer's instructions. The levels of glucose (Shino-Test, Tokyo, Japan) and HbA1c (RAPIDIA Auto HbA1c-L; Fujirebio, Inc., Tokyo, Japan) were determined with whole blood samples. The immunoreactive serum insulin level was determined using a commercial radioimmunoassay kit (Rat insulin RIA kit; Linco Research, Inc., St Charles, MO, USA) with rat insulin as the standard. Systolic blood pressure was measured by the non-invasive tail-cuff method using a manometer–tachometer system (MK-2000, Muromachi Kikai, Tokyo, Japan). The amount of urinary protein excretion for 24 h was determined with TP-HR II Wako reagent (Wako Chemicals). Serum creatinine and urinary creatinine were measured with the creatinine reagent (Alfresa Pharma Corporation, Osaka, Japan), using an automated analyzer (Hitachi-7180, Hitachi High-Technologies, Tokyo, Japan). We calculated the Ccr using the following equation: Ccr (ml min^{-1})=urinary creatinine (mg dl^{-1}) × urine flow rate (ml min^{-1})/serum creatinine (mg dl^{-1}).

Light microscopy

At 30 weeks of age, the anesthetized rats were perfused with 100 ml of saline. For evaluation of light microscopic findings, the kidneys were fixed in 10% paraformaldehyde in PBS (pH 7.4) and finally embedded in paraffin, sectioned, and analyzed for histology. Then, 3-μm sections were subjected to periodic acid-Schiff staining. The mean glomerular tuft volume was determined by the

images from 50 consecutive glomerular cross sections, which were collected for each of the histological sections using an Olympus BX50 light microscope (Olympus, Tokyo, Japan). The area of each glomerular profile was measured manually by tracing the glomerular outline on a computer screen, and the size of each area was calculated by computerized morphometry (Image-Pro plus, Media Cybernetics, Inc., Bethesda, MD, USA). The measurements were performed in a blinded fashion.

Electron microscopy

For transmission electron microscopy, tissues of the left kidneys fixed with 2.5% glutaraldehyde in phosphate buffer (pH 7.4) were postfixed in 2% osmium tetroxide for 2 h at 4 °C. Then, samples were dehydrated in a graded series of ethanol solutions at room temperature, and embedded in Quetol 812 (Nisshin EM Co., Tokyo, Japan). Thin sections of 80 nm were contrasted with 4% uranyl acetate for 15 min and subsequently stained with lead citrate for 5 min at room temperature. Samples were finally examined using a transmission electron microscope (H-7500, Hitachi High-Technologies). The mean width of the GBM was determined by the images of 100 consecutive glomerular sections obtained from two subjects in each group. For scanning electron microscopic examination, small pieces of the kidney cortex were fixed in 2.5% glutaraldehyde in sodium cacodylate buffer (pH 7.4) for 2 h, and subsequently postfixed in 1% osmium tetroxide. Specimens were then dehydrated in a series of ethanols of increasing concentrations, and critical point dried. Once mounted onto specimen holders and desiccated, the samples were sputter-coated with a layer of gold and examined with a S-4300 scanning electron microscope (Hitachi High-Technologies), and images were collected at standard settings.

Immunofluorescent staining

The analysis of nephrin expression in the renal cortex was performed using an immunofluorescence technique. The snap-frozen sections of 3 μm, fixed in 1% formaldehyde and blocked in 5% normal goat serum, were incubated with rabbit anti-nephrin primary antibodies (Immuno-biological Laboratories Co., Ltd., Gunma, Japan) and washed twice with PBS. Subsequently, sections were also incubated with Alexa Fluor 488-conjugated anti-rabbit antibodies (Invitrogen, Carlsbad, CA, USA). Stained sections were examined using a PROVIS AX-80 optical microscope (Olympus). The results were calculated as the intensity of fluorescence within the glomerular tuft by using the Image J 1.42q software package (National Institutes of Mental Health, Bethesda, MD, USA). On average, over 30 randomly selected hilar glomerular tuft cross-sections were assessed per rat.

Statistical analysis

The results were expressed as the means ± s.d. of the mean. The data were analyzed by an analysis of variance combined with Fisher's protected least significant difference. Differences with $P<0.05$ were considered to be statistically significant. The correlation test was used to measure the association between two variables, if appropriate.

CONFLICT OF INTEREST

The authors declare no conflict of interest.

ACKNOWLEDGEMENTS

Part of the work presented in the original manuscript was presented in abstract in the Renal Week 2009 (Annual Meeting of the American Society of Nephrology). We sincerely thank Takashi Yashiro for conducting the electron microscopy studies, and Tom Kouki for his technical assistance in tissue processing for histological and ultrastructural studies.

1 Kambham N, Markowitz GS, Valeri M, Lin J, D'Agati VD. Obesity-related glomerulopathy: an emerging epidemic. *Kidney Int* 2001; **39**: 1498–1509.
2 Ramirez SP, McClellan W, Port FK, Hsu SIH. Risk factors for proteinuria in a large, multiracial, Southeast Asian population. *J Am Soc Nephrol* 2002; **1**: 1907–1917
3 Iseki K, Ikemiya K, Kinjo K, Inoue T, Iseki C, Takishita S. Body mass index and the risk of development of end-stage renal disease in a screened cohort. *Kidney Int* 2004; **65**: 1870–1876.
4 Hallan S, de Mutsert R, Carlsen S, Dekker FW, Aasarod K, Holmen J. Obesity, smoking, and physical inactivity as risk factors for CKD: are men more vulnerable? *Am J Kidney Dis* 2006; **47**: 396–405.
5 Chagnac A, Weinstein T, Herman M, Hirsh J, Gafter U, Ori Y. The effects of weight loss on renal function in patients with severe obesity. *J Am Soc Nephrol* 2003; **14**: 1480–1486.
6 Chen HM, Li SJ, Chen HP, Wang QW, Li LS, Liu ZH. Obesity-related glomerulopathy in China: a case series of 90 patients. *Am J Kidney Dis* 2008; **52**: 58–65.
7 Kasiske BL, Cleary MP, O'Donnell MP, Keane WF. Effects of genetic obesity on renal structure and function in the Zucker rat. *J Lab Clin Med* 1985; **106**: 598–604.
8 Frystyk J, Skjaerbaek C, Vestbo E, Fisker S, Orskov H. Circulating levels of free insulin-like growth factors in obese subjects: the impact of type 2 diabetes. *Diabetes Metab Res Rev* 1999; **15**: 314–322.
9 Wolf G, Hamann A, Han DC, Helmchen U, Thaiss F, Ziyadeh FN *et al.* Leptin stimulates proliferation and TGF-beta expression in renal glomerular endothelial cells. potential role in glomerulosclerosis. *Kidney Int* 1999; **56**: 860–872.
10 Keane WF. Lipids and the kidney. *Kidney Int* 1994; **46**: 910–920.
11 Mu W, Ouyang X, Agarwal A, Zhang L, Long DA, Cruz PE *et al.* IL-10 suppresses chemokines, inflammation, and fibrosis in a model of chronic renal disease. *J Am Soc Nephrol* 2005; **16**: 3651–3660.
12 Yoshioka T, Okada T, Maeda Y, Ikeda U, Shimpo M, Nomoto T *et al.* Adeno-associated virus vector-mediated interleukin-10 gene transfer inhibits atherosclerosis in apolipoprotein E-deficient mice. *Gene Therapy* 2004; **11**: 1772–1779.
13 Hong EG, Ko HJ, Cho YR, Kim HJ, Ma Z, Yu TY *et al.* Interleukin-10 prevents diet-induced insulin resistance by attenuating macrophage and cytokine response in skeletal muscle. *Diabetes* 2009; **58**: 2525–2535.
14 Esposito K, Pontillo A, Giugliano F, Giugliano G, Marfella R, Nicoletti G *et al.* Association of low interleukin-10 levels with the metabolic syndrome in obese women. *J Clin Endocrinol Metab* 2003; **88**: 1055–1058.
15 Coimbra TM, Janssen U, Grone HJ, Ostendorf T, Kunter U, Schmidt H *et al.* Early events leading to renal injury in obese Zucker (fatty) rats with type II diabetes. *Kidney Int* 2000; **57**: 167–182.
16 Kasiske BL, O'Donnel MP, Cleary MP, Keane WF. Treatment of hyperlipidemia reduces glomerular injury in obese Zucker rats. *Kidney Int* 1988; **33**: 667–672.
17 Li MC, He SH. IL-10 and its related cytokines for treatment of inflammatory bowel disease. *World J Gastroenterol* 2004; **10**: 620–625.
18 Ito T, Okada T, Miyashita H, Nomoto T, Nonaka-Sarukawa M, Uchibori R *et al.* Interleukin-10 expression mediated by an adeno-associated virus vector prevents monocrotaline-induced pulmonary arterial hypertension in rats. *Circ Res* 2007; **101**: 734–741.
19 Alderson NL, Chachich ME, Youssef NN, Beattie RJ, Nachtigal M, Thorpe SR *et al.* The AGE inhibitor pyridoxamine inhibits lipemia and development of renal and vascular disease in Zucker obese rats. *Kidney Int* 2003; **63**: 2123–2133.
20 Tsilibary EC. Microvascular basement membranes in diabetes mellitus. *J Pathol* 2003; **200**: 537–546.
21 Caramori ML, Kim Y, Huang C, Fish AJ, Rich SS, Miller ME *et al.* Cellular basis of diabetic nephropathy: 1. Study design and renal structural-functional relationships in patients with long-standing type 1 diabetes. *Diabetes* 2002; **51**: 506–513.
22 Akimoto T, Ito C, Saito O, Takahashi H, Takeda S, Ando Y *et al.* Microscopic hematuria and diabetic glomerulosclerosis—clinicopathological analysis of type 2 diabetic patients associated with overt proteinuria. *Nephron Clin Pract* 2008; **109**: c119–c126.
23 Fürnsinn C, Komjati M, Madsen OD, Schneider B, Waldhäusl W. Lifelong sequential changes in glucose tolerance and insulin secretion in genetically obese Zucker rats (fa/fa) fed a diabetogenic diet. *Endocrinology* 1991; **128**: 1093–1099.
24 Sandler S, Welsh N. Interleukin-10 stimulates rat pancreatic islets *in vitro*, but fails to protect against interleukin-1. *Biochem Biophys Res Commun* 1993; **195**: 859–865.
25 Sarafidis PA, Ruilope LM. Insulin resistance, hyperinsulinemia, and renal injury: mechanisms and implications. *Am J Nephrol* 2006; **26**: 232–244.
26 Bjorn SF, Bangstad HJ, Hanssen KF, Nyberg G, Walker JD, Viberti GC *et al.* Glomerular epithelial foot processes and filtration slits in IDDM patients. *Diabetologia* 1995; **38**: 1197–1204.
27 Herbach N, Schairer I, Blutke A, Kautz S, Siebert A, Goke B *et al.* Diabetic kidney lesions of GIPR^{dn} transgenic mice: podocyte hypertrophy and the thickening of the GBM precede glomerular hypertrophy and glomerulosclerosis. *Am J Physiol Renal Physiol* 2009; **296**: F819–F829.
28 Bonnet F, Cooper ME, Kawachi H, Allen TJ, Boner G, Cao Z. Irbesartan normalizes the deficiency in glomerular nephrin expression in a model of diabetes and hypertension. *Diabetologia* 2001; **44**: 874–877
29 Luimula P, Ahola H, Wang SX, Solin ML, Aaltonen P, Tikkanen I *et al.* Nephrin in experimental glomerular disease. *Kidney Int* 2000; **58**: 1461–1468.
30 Hollis JH, Lemus M, Evetts MJ, Oldfield BJ. Central interleukin-10 attenuates lipopolysaccharide-induced changes in food intake, energy expenditure and hypothalamic Fos expression. *Neuropharmacology* 2010; **58**: 730–738.
31 Okada T, Nomoto T, Yoshioka T, Nonaka-Sarukawa M, Ito T, Ogura T *et al.* Large-scale production of recombinant viruses by use of a large culture vessel with active gassing. *Hum Gene Ther* 2005; **16**: 1212–1218.

Recovery of neurogenic amines in phenylketonuria mice after liver-targeted gene therapy

Hiroya Yagi[a,b], Sho Sanechika[c], Hiroshi Ichinose[c], Chiho Sumi-Ichinose[d], Hiroaki Mizukami[a], Masashi Urabe[a], Keiya Ozawa[a] and Akihiro Kume[a]

Phenylketonuria (PKU) is a common genetic disorder arising from a deficiency of phenylalanine hydroxylase. If left untreated, the accumulation of phenylalanine leads to brain damage and neuropsychological dysfunction. One of the abnormalities found in hyperphenylalaninemic patients and a mouse model of PKU is an aminergic deficit in the brain. We previously showed correction of hyperphenylalaninemia and concomitant behavioral recovery in PKU mice after liver-targeted gene transfer with a viral vector. Here, we addressed whether such a functional recovery was substantiated by an improved amine metabolism in the brain. After gene transfer, brain dopamine, norepinephrine, and serotonin levels in the PKU mice were significantly elevated to normal or near-normal levels, along with systemic improvement of phenylalanine catabolism. The results of biochemical analyses validated the efficacy of PKU gene therapy in the central nervous system. *NeuroReport* **23:30–34 © 2011 Wolters Kluwer Health | Lippincott Williams & Wilkins.**

NeuroReport 2012, **23**:30–34

Keywords: catecholamine, gene therapy, phenylketonuria, serotonin

[a]Division of Genetic Therapeutics, Jichi Medical University, Shimotsuke, [b]Department of Obstetrics and Gynecology, Institute of Clinical Medicine, University of Tsukuba, Tsukuba, [c]Department of Life Science, Graduate School of Bioscience and Biotechnology, Tokyo Institute of Technology, Yokohama and [d]Department of Pharmacology, School of Medicine, Fujita Health University, Toyoake, Japan

Correspondence to Dr Akihiro Kume, MD, PhD, Division of Genetic Therapeutics, Jichi Medical University, 3311-1 Yakushiji, Shimotsuke, Tochigi 329-0498, Japan Tel: +81 285 58 7402; fax: +81 285 44 8675; e-mail: kume@jichi.ac.jp

Received 1 September 2011 **accepted** 17 October 2011

Introduction

Phenylketonuria (PKU; OMIM 261600) is a common inherited metabolic disorder, mostly arising from a deficiency of phenylalanine hydroxylase (PAH) [1]. PAH is exclusively responsible for converting phenylalanine into tyrosine, and its deficiency results in a systemic accumulation of phenylalanine in the body. Although the mechanisms involved are not fully understood, excessive amounts of phenylalanine are toxic to the developing brain and have a negative impact on neuropsychological function in adults. Therefore, the present treatment for PKU mandates strict restrictions of dietary protein in infancy and childhood to limit phenylalanine intake, and a similar diet is recommended for life. One possible mechanism responsible for the neurological dysfunction is an aminergic deficit, as earlier studies showed drastic decreases in neurotransmitters such as dopamine, norepinephrine, and serotonin (5-hydroxytryptamine, 5-HT) in the brains of untreated PKU patients [2,3]. A similar aminergic deficit was found in a mouse model of PKU (the *Pah*^{enu2} strain) [4–7]. We and other investigators have explored the feasibility of somatic gene therapy for PKU, and have shown that recombinant adeno-associated virus (AAV) vectors can achieve long-term corrections of hyperphenylalaninemia (HPA) in *Pah*^{enu2} mice [8–10]. We also demonstrated a behavioral recovery in the treated animals, indicating that some brain functions benefited from this approach [8]. In the present study, we addressed whether liver-targeted gene therapy for PKU would reinstate the metabolism of neurogenic amines, thereby improving homeostasis and the function of the central nervous system.

Materials and methods

Animals

All the animal experiments were carried out in accordance with the institutional guidelines under protocols approved by the Institutional Animal Care and Use Committee at Jichi Medical University (Shimotsuke, Japan). PAH-deficient C57BL/6-*Pah*^{enu2} mice (PKU mice, −/−) were homozygous for the same *Pah*^{enu2} mutation as that described in the original BTBR-*Pah*^{enu2} strain [4,5], but had been bred and backcrossed on the C57BL/6J background. Genotyping for the presence of the *Pah*^{enu2} mutation was performed by PCR analysis of tail biopsy DNA [9]. All the mice were maintained on standard mouse chow (CE-2 from Clea, Tokyo, Japan). Blood was collected from the tail veins on a filter paper for newborn mass screening (No. 545 from Advantec Toyo, Tokyo, Japan), and blood phenylalanine concentrations were determined by an enzymatic fluorometric assay using an Enzaplate PKU-R kit (GE Healthcare, Tokyo, Japan) and a Fluoroskan Ascent FL plate reader (Labsystems, Helsinki, Finland) [8,9]. *In-vivo* phenylalanine oxidation was evaluated by a noninvasive breath test using [1-^{13}C]L-phenylalanine [9,11].

In-vivo gene transfer

The construction and preparation of the AAV8-pseudotyped self-complementary AAV vector for PKU (scAAV8/

0959-4965 © 2011 Wolters Kluwer Health | Lippincott Williams & Wilkins DOI: 10.1097/WNR.0b013e32834e3a87